Fuel 405 (2026) 136572

Contents lists available at ScienceDirect

Fuel

journal homepage: www.elsevier.com/locate/fuel

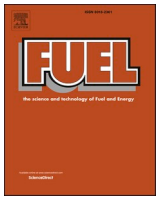

Full Length Article

A semi-detailed chemical kinetic model of polybutadiene pyrolysis

Lauren T. Creadore [a], Andrea Locaspi [b], Tricia M. Marchese [a], Matteo Pelucchi [b], Tiziano Faravelli [b], Marco J. Castaldi [a,*]

[a] Combustion and Catalysis Laboratory – Department of Chemical Engineering, The City College of New York, USA
[b] CRECK Modeling Lab – Department of Chemistry, Materials and Chemical Engineering, Politecnico di Milano, Italy

A B S T R A C T

Polybutadiene (PB) is an important polymer with various applications including next-generation solid fuel propellants. Understanding its pyrolysis behavior under various conditions is essential for tuning to these applications. In this study, pyrolysis of polybutadiene with a well-defined 20 % vinyl and 80 % cis + trans composition is investigated using thermogravimetric analysis at heating rates from 10 °C min^{-1} to 100 °C min^{-1}. Gas speciation was measured via py-GC/MS to identify and quantify products. The CRECK condensed-phase kinetics framework for polymer pyrolysis is extended to predict decomposition mechanisms and product distributions of PB. The model incorporates 50 species and 415 reactions.

Experimental results reveal two distinct decomposition steps occurring at 350 °C and 475 °C across all investigated heating rates, responsible for 5 wt% and 95 wt % loss, respectively. The model reproduces mass loss profiles to within 6 wt% accuracy, though early decomposition stages show deviations attributed to the exclusion of cis–trans isomerization reactions. An important result is the primary production of 4-vinylcyclohexene from 0 to 5 % mass loss, butadiene after 5 % mass loss, followed by dimers and trimers respectively in order of net rates of production of gas phase species. Predictions of chemical product speciation capture the butadiene to 4-vinylcyclohexene ratio, and the butadiene to five-carbon cyclic species ratio from an average of literature sources to within 55 % and 37 % respectively. This work provides new, high-quality experimental data, including the measurement of 34 gaseous products, and an extended kinetic framework, advancing the understanding of PB thermal degradation and supporting its application in thermal recycling and advanced energetic materials.

1. Introduction

The thermal decomposition of polybutadiene (PB) has garnered significant attention with respect to environmental solutions to end-of-life plastic and rubber products. While recycling rates in the U.S. have improved from 11 % in 1990 to 79 % in 2024, and tire stockpile mass has reduced by 95 % in the same period, the U.S. still generates 3.8 million tons of tire waste annually [1]. Thermal conversion offers a pathway to produce feedstock olefins and monomers from PB, reducing virgin resource demand. One of the primary synthetic rubber components in tires is synthesized from polybutadiene [2]. Therefore, attempts to valorize waste tires thermally require an understanding of the rubber components during decomposition. Importantly, major chemical companies are developing polymer pyrolysis technologies to scale these efforts [3–5].

Another essential aspect of understanding solid polymer decomposition is in the realm of propellant fuel development. Degradation chemistry of the solid propellant directly determines the composition of the gas-phase from which combustion properties such as flame speed and ignition delay, as well as thermal properties, depend. Hydroxyl-terminated polybutadiene (HTPB) is the most widely used binder in solid composite propellants, serving as the primary polymer matrix to which additives are incorporated to tailor reaction properties [6]. Recent research has explored reactive metal enhancers for the development of next generation solid fuels [7]. Experimental research efforts have focused on measuring key parameters such as heat release rates, evolved gaseous species, melt temperatures, and overall regression rates [8–11]. These data are critical to ensuring that solid fuels meet the demands of supersonic flight by withstanding extreme mechanical loads while providing the necessary thrust and burn duration. Experimental measurements provide essential data for correlation development, and a complementary fundamental understanding of polymer decomposition is necessary to inform additive selection to improve key performance parameters. While HTPB is the industry standard, this study focuses on polybutadiene as a model polymer to investigate fundamental decomposition mechanisms. PB and HTPB share the same repeating monomer units, differing only by the hydroxyl end groups in HTPB. Investigating PB, a simpler yet chemically analogous polymer, allows for a detailed mechanistic analysis of the main degradation pathways that should govern both materials. Notably, the most used HTPB formulation for solid propellants, R45M [12], contains 20 wt% vinyl content. This study presents the first mass loss experimental data for pure PB at 20 wt%

* Corresponding author at: 160 Convent Avenue, ST 307, New York, NY 10031, USA.
E-mail address: mcastaldi@ccny.cuny.edu (M.J. Castaldi).

https://doi.org/10.1016/j.fuel.2025.136572
Received 15 April 2025; Received in revised form 7 July 2025; Accepted 18 August 2025
Available online 29 August 2025
0016-2361/© 2025 Elsevier Ltd. All rights are reserved, including those for text and data mining, AI training, and similar technologies.

vinyl, highlighting its relevance for practical applications.

An extensive literature survey has revealed that even for a well-known and highly studied polymer such as polybutadiene, there is a considerable range of variability in thermal decomposition data. A pyrolysis study was conducted by Choi & Han [13] for commercial grade, 98 % cis 1,4 polybutadiene at temperatures between 540–860 °C. The gaseous chemical species identified were of carbon number C_4, C_5, C_6, C_7 and C_8 and were presented as relative ratios. Those ratios were used to support proposed decomposition process, yet absolute quantities of each were not reported. The pyrolysis of the elastomer constituents of waste tires was done by Lah et al. [14] in a temperature range of 500–700 °C using thermogravimetric analysis (TGA) and differential scanning calorimetry (DSC). The data obtained were simulated using a model that included internal heat transfer combined with an n^{th} order kinetic model. The authors determined the kinetic parameters and found the reaction order for the constituents ranged from 0.86 to 1.7. Another pyrolysis study using the polymeric fraction intended for tires was done by Menares et al. [15] using TGA and pyrolysis–gas chromatography-mass spectrometry (py-GC/MS). Gaseous chemical species identified were light gases, cyclic hydrocarbons, and aromatics, reported as a function of temperature. The authors used a power-law model and a combined Flynn-Wall-Ozawa, Kissinger-Akira-Sunose model to propose that a Diels-Alder cyclization process was responsible for the measured limonene and isoprene. Therefore, this work presents new pyrolysis data using a well-defined polybutadiene (20 % vinyl, 80 % cis and trans microstructure) over a range of relevant heating rates (10 to 100 °C min^{-1}) appropriate for supersonic flight applications. The data obtained from the TGA measurements include identification of 34 gaseous chemical species across four temperatures as a function of PB decomposition. Besides extending and complementing the available experimental information on PB degradation, this work presents a high-fidelity model providing sufficient insights to guide both demands in the area of space propulsion (e.g., required reactive additives for flight trajectory) and chemical reactor design (e.g., for end-of-life polymer processing).

This model is, to the best of the authors' knowledge, the first one in the literature overcoming single step empirical approaches for PB, extending the CRECK kinetic framework for plastic polymer pyrolysis [16], and allowing a mechanistic understanding and interpretation of the impact of heating conditions and feedstock characteristics on degradation features and products distribution. Few models have been developed to simulate the pyrolysis of pure polybutadiene [17,18]. More generally than PB as a target feedstock, models have been developed for functionally terminated polybutadiene (e.g., HTPB) in either a mixture [19] or in a copolymer [20]. Most broadly, models exist for similar polymers (e.g., polyethylene) as either a standalone component [21], in a copolymer (e.g., as used in tires) [22], or in a composite material [23].

To simulate plastic pyrolysis, global kinetic models are generally more prevalent than semi-detailed kinetic models [24]; this was found to be the case for PB specifically as well. Some global models employ one-dimensional lumped multi-step reactions derived from TGA apparent kinetics [20,23]. Other models, including one for the pyrolysis of an HTPB and ammonium perchlorate (AP) compounds [19], employ a single-step approach. In that study [19], the decomposition of HTPB alone, omitting interaction with AP and its decomposition products, was included as a component of the kinetic scheme. The modeled decomposition of HTPB was limited to a single global reaction step, yielding predominantly the monomer, as well as small concentrations of methane and hydroxyl radicals to account for the functional groups on the starting polymer. Burning rates of the HTPB/PB mixture were validated with experimental data, yet predicted gas speciation was not validated. Less prevalent than the lumped models are more detailed models, such as one applied to pure polybutadiene pyrolysis which was simulated in a reactive molecular dynamics ReaxFF simulation [17]. The molecular dynamics simulation employed a 40-monomer chain model compound containing both 1,2 and 1,4 moieties, incorporated kinetics by way of apparent activation energies derived from TGA, and was validated by TGA and py-GC/MS, though at vastly lower temperatures and heating rates than the simulation. Other researchers took a lumped kinetic modeling approach to the pyrolysis of pure polybutadiene based on the pyrolysis of tire rubber [18]. That approach employs three main kinetic schemes, each with four or fewer lumped kinetic parameters. Mass and heat transfer considerations, and the effect of self-heating and self-cooling effects were novel contributions to that model. Simulated mass loss profiles were validated by TGA experiments. By design, that model does not predict product species. Lacking in the existing set of models is a detailed or semi-detailed kinetic model to overcome the simplifications introduced by global apparent-kinetics or an overly reduced set of reactions which is validated at relevant conditions. The new model proposed in this work is developed with sufficient detail to predict both mass loss and product speciation, with a robust set of products to accurately describe the decomposition, including behavior (e.g., crosslinking) at low temperatures prior to the onset of mass loss.

2. Materials and methods

2.1. Experiment

Thermogravimetric analysis and differential scanning calorimetry were performed using a TA SDT650 TGA/DSC under ultra-high-purity nitrogen gas (TW Smith, UHP 5.0 purity) supplied at a flow rate of 50 mL min^{-1}. Polybutadiene (Millipore Sigma #383694) was selected for its well-characterized properties (number average molecular weight ~ 5,000 g mol^{-1}), with a microstructural composition of 80 % cis and trans, 20 % vinyl.

The current study prioritizes small initial sample masses to reduce heat transfer effects and ensure high fidelity data. The minimum starting mass of liquid polybutadiene samples was 5.7 mg, yet masses up to 11.0 mg were evaluated and produced high-accuracy results. Average values of triplicate experiments are reported in section 3.1.1 with the largest standard deviation near 10 %. The experiments were performed over a range of heating rates, from 10 °C min^{-1} to 100 °C min^{-1}, to elucidate the influence of heating rate on reaction pathways and the distribution of pyrolysis products. The TG heating procedures were as follows: 25 °C initial temperature heated at a constant rate of 10, 30, 60 or 100 °C min^{-1} until a final temperature of 570 °C for the lowest heating rate up to 660 °C for the highest heating rate to ensure the test temperature exceeded the final decomposition temperature. The samples were placed in 100 μ L alumina pans with a pan height-to-diameter ratio of 0.7. This aspect ratio, combined with the horizontal purge gas flow, ensured rapid removal and quenching of evolved gases, minimizing the likelihood of secondary reactions [25]. The TGA instrument used is configured with the balance arm upstream of the evolved gas flow, preventing possible condensation of evolved gases on the balance arm, which could otherwise impact apparent mass measurements.

Py-GC/MS was performed to identify and quantify the gaseous species produced from pyrolysis of pure polybutadiene. The GC/MS system (Agilent GC 7890B, Agilent MS 5977A) was directly connected to the outlet of the TGA via a heated, passivated transfer line, and was equipped with a Shimadzu SHR5XLB, 30 m × 0.25 mm inner diameter, 0.25 μm film thickness capillary column. The carrier gas was helium 3.0 UHP (supplied by Airgas) at a constant flow of 1.1482 mL min^{-1}. The valve box heater was held at 225 °C.

The GC oven temperature program was as follows: initial hold at 60 °C, followed by a ramp to 66 °C at 0.5 °C min^{-1} with a hold for 1.0 min, a ramp to 70 °C at 1.0 °C min^{-1}, a ramp to 80 °C at 5.0 °C min^{-1}, a ramp to 255 °C at 30 °C min^{-1}, with a final hold for 3.0 min. The MS operated in electron ionization mode at 70 eV, scanning from 10 to 550 *m/z*. The ion source and quadrupole temperatures were maintained at 230 °C and 150 °C, respectively.

Compounds were identified by comparing mass spectra to entries in the NIST V11 library and by matching retention times to reference standards when available. Quantification was performed using three-to-

four-point calibration curves generated from standard compounds representative of key pyrolysis products (n-pentane for linear hydrocarbons and p-xylene for cyclic hydrocarbons). For compounds in which direct calibration was not employed, quantification relied on published electron impact ionization cross sections [26,27] for the same or structurally analogous compounds. This approach enabled accurate estimation of the absolute mass of evolved products, accounting for compound-specific detector response and allowing direct comparison across experiments.

2.2. Kinetic mechanism

This work introduces the first semi-detailed chemical kinetic mechanism capable of predicting both the PB decomposition mass profiles and its resulting products, representing a significant advancement in polymer pyrolysis modeling. This study builds upon the semi-detailed kinetic model from Locaspi et al. [28] to simulate the primary condensed-phase reactions involved in PB pyrolysis. The model captures the major decomposition pathways that dominate the process, providing a fundamental understanding of PB degradation. Despite being relatively small in size as a result of the functional group approach by Locaspi et al. [28], (i.e., incorporating only 50 gas + liquid chemical species and 415 condensed-phase reactions), the model effectively captures the key decomposition characteristics of PB, including mass loss profiles and major product speciation, balancing complexity and capability of providing valuable insights into the dominant chemical degradation pathways.

The model focuses on molten-phase reactions occurring for a PB material that was liquid at standard temperature and pressure, and on the formation of primary degradation products. Homogeneous liquid-phase reactions constitute the primary degradation mechanism, and evaporation is treated through volumetric pseudo-reactions [29]. Secondary reactions in the gas phase of evolved species, which may be relevant in practical applications such as pyrolysis/gasification reactors and combustion systems, are not considered in this work. Yet, the model correctly predicts the complete conversion of PB without residue, consistent with experimental findings in the literature [18,30,31]. The full CHEMKIN-format mechanism is available on the CRECK Modeling Lab GitHub repository[1] and is attached as Supplementary Material (SM) to this work.

The reaction mechanism relies on analogies with gas-phase degradation pathways and established molecular pathways. Bond dissociation energies from the ATcT [32] and NIST [33] databases and published literature [34] are used for rate constant estimation, with an approach that can be extended to compounds containing similar bonds. Evaporation reactions are estimated based on the boiling temperatures and vapor pressures computed through the group contribution methodology by Nannoolal et al. [35,36].

2.2.1. Species description

In this study, the functional group approach is employed to model an ideal polybutadiene polymer, representing polymer chains as pseudo-species composed of mid-chain (MC) and end-chain (EC) moieties, attributing reactivity to the functional groups alone. High molecular weight (HMW) polymeric chains are represented with this simplified description, while low molecular weight (LMW) compounds of interest (e.g., butadiene) are represented with real species and associated physical properties, such as boiling point. The pseudo-species employed to represent HMW chains capture the primary reactive sites and molecular structure and preserve chain lengths, closing an elemental mass balance. These functional groups enable tracking of molecular weight distribution and ensuring of physical consistency by considering neighboring fragments, termed supporting polymer units (SPUs). These SPUs allow for a simple and generalizable way to represent the polymer chain to which the functional group of interest is bound. Rather than establish every possible permutation of polymer chain length, all with the same functional group and differing only by the degree of polymerization, implementation of the SPUs accounts for the remaining chain length after reaction. In this way, complexity of the model is reduced while information about the polymer chain length is retained. Further details can be found in previous works [28,29,37].

The microstructure of polybutadiene, as shown in Fig. 1, consists of three primary units: the 1,4-cis and 1,4-trans moieties, where the double bond is incorporated into the polymer backbone, and the 1,2-vinyl moiety where, in contrast, the double bond exists in the vinyl ligand attached to the polymer backbone. The model introduces microstructure-specific reaction mechanisms and reaction parameters to account for differences in the chemistry between these structures. Notably, the 1,2-vinyl structure contains both secondary and tertiary carbons, whereas the 1,4 structures consist solely of secondary carbons. Additionally, the 1,2-vinyl configuration can exhibit tacticity (isotactic, syndiotactic, or atactic arrangements), a stereochemical feature not present in the 1,4 configurations. The presence of the double bond within the backbone of the 1,4 configurations restricts rotational freedom due to the inability to rotate around double bonds, impacting the polymer's conformational mobility and overall flexibility. These features impact polymer degradation and have previously been explored for PB specific crosslinking reactions [38] and polymerization reactions [39].

In this work, cis and trans isomers are combined into a single 1,4 moiety, effectively simplifying the microstructural representation by omitting stereospecific distinctions between the structures. This lumping simplification is justified by studies indicating that product speciation remains relatively insensitive to the cis:trans ratio when the trans content is below 60 wt% [40,41]. One study reports that with trans content above 60 wt%, increased selectivity for five-membered cyclic products at the expense of 4-vinylcyclohexene by up to 13 wt% occurs at low conversions, suggesting an influence of stereospecificity on speciation at high trans content, though the reason for this is not thoroughly elucidated [40]. In addition, the stability of the repeating units for the cis-isomer is between 1.5 – 2 kcal mol^{-1} lower than the trans-isomer, yet the onset temperature of decomposition is within 15 °C of each other because the main processes for decomposition are the C–C chain sessions and random backbone degradation. However, that observation stands in contrast to a more extensive multi-manufacturer study which tested low initial mass (<2 mg) samples and found no significant speciation differences between high-cis and high-trans PB [42]. Therefore, lumping cis and trans isomers into a single 1,4 moiety is considered appropriate for feedstocks spanning a wide range of microstructural composition for modeling purposes. As cis and trans moieties are not explicitly distinguished, cis–trans isomerization [43] is necessarily excluded from the model.

Important reactive rates such as hydrogen abstraction and C–C scission are similar between cis and trans microstructures [34,44]. Yet, differences in rotational barriers and stereospecificity may influence reactions such as Diels-Alder cyclization, particularly in the formation of 4-vinylcyclohexene via intermolecular addition and crosslinking phenomena [45–47]. Distinguishing between the cis and trans moieties enables predicting variation in stereospecific reaction pathways affect

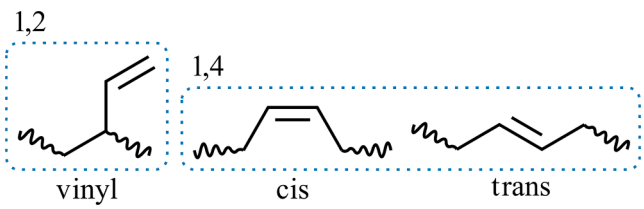

Fig. 1. Polybutadiene microstructures with lumping of 1,4 moieties.

[1] https://github.com/CRECKMODELING/Kinetic-Mechanisms/.

speciation and mass loss, albeit at higher computational cost. Conversely, the 1,2 vinyl moiety is retained as a distinct microstructural unit to accurately capture the unique chemical characteristics and reactivity associated with its pendant vinyl group.

The structural differences between 1,4-butadiene and 1,2-butadiene units are explicitly represented in the model through distinct pseudo-species. The adopted nomenclature designates 1,2 units with a terminal "v" to differentiate them from their 1,4 counterparts. The base pseudo-species, representing a polymer fragment composed of four repeating 1,4-butadiene units, is named P-PB-P, while its 1,2-butadiene analog is designated as P-PBv-P. The distinction between 1,4 and 1,2 units is retained also in the end-chain pseudo-species, but not for LMW products, allowing to significantly decrease the number of species and reactions. The model also considers the crosslinked 1,4 and 1,2 mid-chain units, denoted by the "x" in their name (e.g., P-PBx-P). All polymer species are identified by the initial "P-" in their label representing their bonds with the rest of the network, with mid-chains having also a terminal "-P". To distinguish condensed-phase species from gas-phase ones, a suffix "(L)" is appended to the names of the former. Representative examples of HMW end- and mid-chain structures, and LMW degradation products are summarized in Table 1, along with the total number of each species included in the model.

While the proportions of the three microstructures present in a given PB sample are often well-defined, characterization of and confidence in the monomer sequence distribution is not consistent [48–51]. It is not clear whether all moieties of a certain type exist in uninterrupted blocks or rather are interspersed among the other units. This uncertainty has likely led some prior studies to assume random distributions of monomer units [51,52]. Given these ambiguities, a simplified approach is adopted in this work to describe vinyl content distribution. For PB samples with a vinyl content of $\leq$ 10 wt%, all vinyl groups are assumed to be isolated (i.e., flanked by 1,4 structures). For compositions with vinyl content $>$ 10 wt% and $\leq$ 30 wt%, half of the vinyl moieties are assumed to be isolated, with the remainder forming continuous, uninterrupted blocks. At higher vinyl contents, with compositions $>$ 30 wt% and $\leq$ 50 wt%, the fraction of isolated vinyl units decreases to 25 %, while for samples containing $>$ 50 wt% and $\leq$ 70 wt% vinyl, only 10 % of the vinyl groups are assumed to be isolated. Finally, for polymers exceeding 70 wt% vinyl content, there are no 1,2 structures assumed to be isolated.

To represent key radical degradation pathways, the model considers resonantly stabilized radicals, which are mainly secondary allylic on 1,4 microstructures and tertiary allylic on 1,2 microstructures (shown as products of reactions R1 and R1v in Fig. 2). Species containing internal radicals (denoted by the "_i" within their labels) are key intermediates in forming oligomers, while those containing terminal radicals (denoted by the "_t" in their label) preferentially yield butadiene, 4-vinylcyclohexene (labelled VCH), dimers and trimers. A comprehensive figure depicting all reactant species included in the model as well as additional reaction pathways can be found in the Supplemental Materials Fig. S1.

Prior studies [40,53–55] identified the most abundant PB pyrolysis products and those of similar diene polymers, such as HTPB [43,56–58], its copolymers [59,60], and its rubbers [30,61,62]. From these studies, compounds with yields above 4 wt% are incorporated in the current description, with product distributions from the literature informing the definition of reaction pathways in the condensed phase. Importantly, Diels-Alder and cyclization reactions of the evolved species can occur in the gas phase [63], which may hinder the accurate measurement of primary pyrolysis products, motivating the use of spectroscopic methods close to the burning surface [64] or quenching [43], as in previous studies. Therefore, the simulated results must be compared to appropriate corresponding experimentally-measured speciation data at conditions and in configurations that limit secondary gas phase reactivity.

Lumping [65] is applied to simplify the mechanism, grouping oligomers by carbon number (e.g., all trimers, cyclic or aliphatic), except for 4-vinylcyclohexene, which, due to its high abundance, is treated separately with a dedicated reaction scheme. Species lumping introduces a small error of approximately 5 wt%. For example, small species used solely for atom balancing (e.g., C_2H_2) represent only up to 1.5 wt% of the total products and are not treated as true pyrolysis products. Similarly, real pyrolysis products reported in the literature, such as toluene (e.g., from HTPB [56,57]), are not explicitly included in the model through formation pathways nor from delumping, and are possibly formed by secondary gas-phase degradation and isomerization outside the scope of this study. Species with a boiling temperature lower than 250 °C are assumed to form directly in gas-phase upon stabilization because of their high boiling rates. Conversely, the model accounts also for the condensed-phase reactivity of the tetramer and longer oligomers [31] but, to reduce the computational cost, the C_{16+} carbon distribution is represented only through the tetramer and heptamer by the lever rule [16].

2.2.2. Polymer backbone degradation mechanism

Polybutadiene decomposes following a radical degradation mechanism similar to other polyolefins [66], as briefly reiterated in the present section and sketched in Fig. 2. Nevertheless, the unsaturation along the backbone chain enables polymer-specific reaction pathways as discussed in section 2.2.3. Backbone degradation of PB is initiated through random chain scission (reactions R1, R1v in Table 2) at elevated temperatures, typically starting at ~ 350–400 °C [67]. This degradation is initiated by the cleavage of C–C bonds along the backbone, producing reactive intermediates. These random scissions generate radicals that can propagate or terminate through recombination. Similarly to other vinyl polymers, the propagation reactions considered are hydrogen abstraction (R2, R2v), beta-scission (R3, R3v), unzipping (R4, R4v), and backbiting (R5, R5v). Further, radical addition cyclization reactions

Table 1
Schematic representation of the HMW and LMW species introduced for PB degradation.

Species type		Total # of species in model		Representation of select main species
		Stable species	Radical species	
HMW	MC	5	4	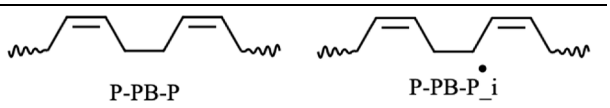
	EC	4	5	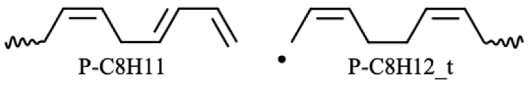
LMW		15	16	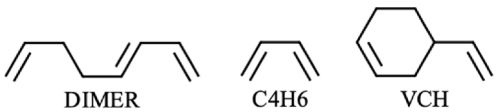

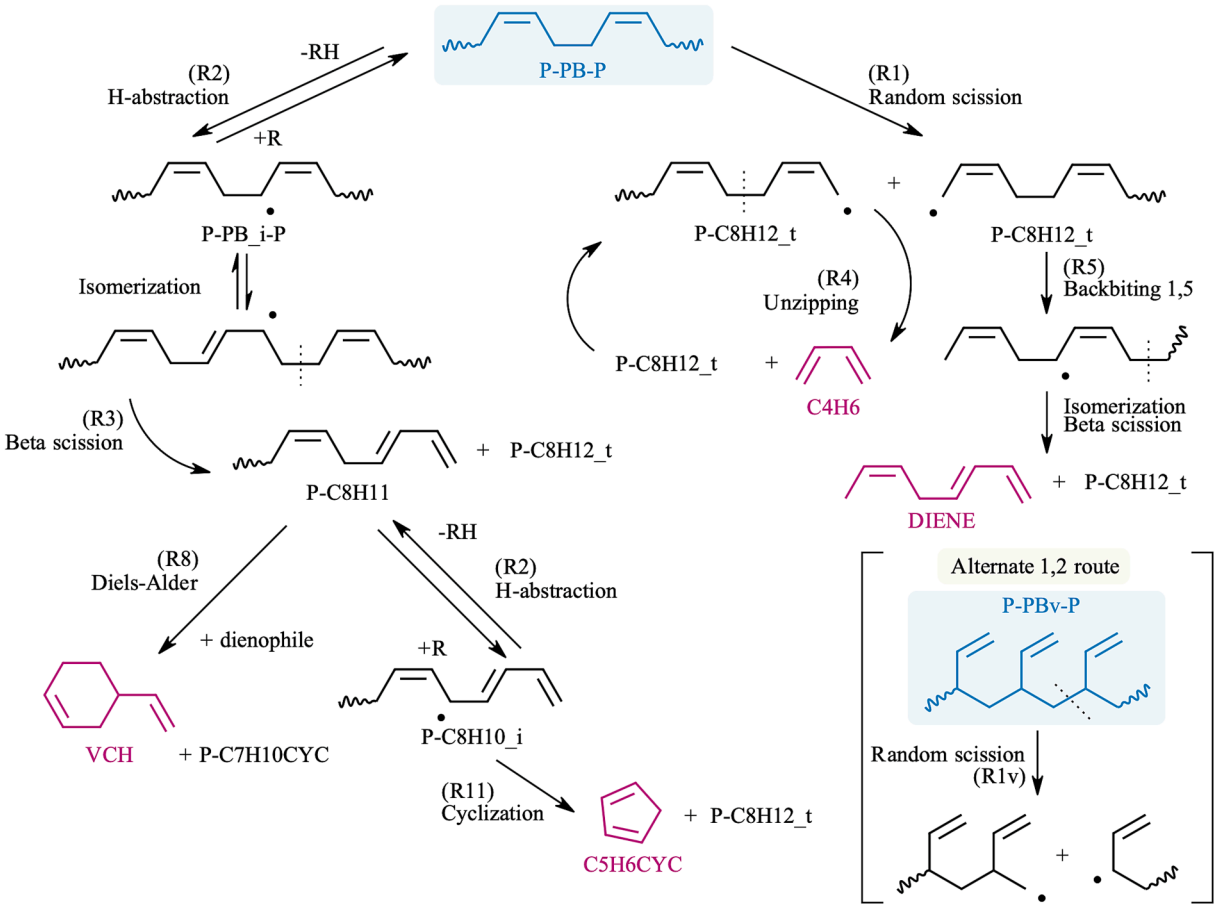

Fig. 2. Schematic representation of the main pathways in polybutadiene (blue) degradation mechanism through molecular and radical reactions to form major products (purple). (For interpretation of the references to color in this figure legend, the reader is referred to the web version of this article.)

(R10, R11) are also considered as discussed in the section 2.2.3.

Chain scission along the polymer backbone (R1 and R1v) forms terminal radicals, which can either decompose (e.g., by unzipping or by intramolecular isomerization followed by beta-decomposition) or stabilize (e.g., by intermolecular H-transfer on any stable species forming internal radicals). A notable pathway involves hydrogen abstraction from polybutadiene MC moieties, followed by beta-scission (R2 and R3), generating a terminal allylic radical and a stable diene. Similarly, abstraction on end-chain species form internal radicals that decompose to release oligomers and terminal radicals. The formation of these aliphatic dimers, trimers, and oligomers up to carbon number 28 are modeled as forming in a single lumped step, with equal probability. The dienes formed by beta-scission reactions also decompose by hydrogen abstraction followed by beta-scission to preferentially release an unsaturated dimer labelled C_8H_{10}. Termination reactions in the model follow the approach of Locaspi et al. [28], occurring exclusively via radical–radical recombination. These reactions increase average chain length and are modeled as combinations of MC and EC moieties to avoid introducing additional species that do not affect the overall degradation.

The models for the 1,4 and 1,2 microstructures are similar, but specific deviations both in reaction pathways and rate parameters are introduced. Specifically, terminal radicals of the vinyl moieties can undertake 1–5 backbiting analogously to other vinyl polymers [66]. This reaction is an intramolecular hydrogen transfer through a six-member transition state, which results in the formation of a more stable internal radical. The decomposition of this radical for the 1,2 microstructure then results in preferential formation of the trimer and heptadienyl radicals (C_7H_{11}), as shown in Fig. 3. The same reaction can take place also on 1,4 microstructures, in that case, resulting in the preferential formation of the dimer only. In both cases, a single lumped reaction is introduced to represent this process, assuming that the isomerization is the rate-determining step analogously to other vinyl polymers [66].

2.2.3. *Polybutadiene-specific degradation mechanisms*

Beyond the radical backbone degradation, the availability of double bonds along the polymer chains enables additional reaction pathways that contribute significantly to the thermal decomposition of PB. These include crosslinking, intramolecular cyclization, and decomposition of specific functional groups. These reaction classes play a critical role in determining product speciation, particularly in the formation of cyclic species such as 4-vinylcyclohexene and other five-member cyclic hydrocarbons.

Crosslinking is among the most important reactions occurring within the polymeric melt below the decomposition temperature. This process leads to the formation of a branched network characterized by reduced unsaturation, without significant variation in polymer mass. In the present work, crosslinking is explained through ene reactions (R6), in line with the experimental observation of Golub [46], which converts the original polymer into branched units as shown in Fig. 4. Furthermore, the reaction enthalpy of approximately –22 kcal mol^{-1} explains the exothermicity observed in the early stage of PB decomposition, both in this work and in previous studies [31,54,67,68]. To simplify the reaction mechanism, only the 1,2–1,2 and 1,4–1,4 crosslinked structures are considered, while the mixed conformation is represented as equimolar average of the other two. The two crosslinks share several similarities, such as the reduced number of allylic hydrogens and formation of alkyl, but they also exhibit opposite effects on polymer degradation. Specifically, the 1,4-crosslink loses four diallylic structures, converting

Table 2
Modified-Arrhenius parameters for the rate constants of elementary reactions (units cm, mol, s, cal). $k = A\ T^{n_A}\ \exp(-E_{act}R_g^{-1}T^{-1})$.

Reaction		A	n_A	E_{act}
R1	Diallylic random scission	2.00×10^{12}	0	54,000
R1v	Allylic random scission	2.00×10^{13}	0	67,000
R2	Hydrogen abstraction (from 1,4 by secondary carbon)	7.50×10^{10}	0	18,000
R2v	Hydrogen abstraction (from tertiary 1,2 by secondary carbon)	4.00×10^{10}	0	16,200
R3	Beta-scission (1,4)	3.00×10^{13}	0	29,000
R3v	Beta-scission (1,2)	3.00×10^{13}	0	28,000
R4	Unzipping (1,4)	2.00×10^{13}	0	26,000
R4v	Unzipping (1,2)	2.00×10^{13}	0	25,000
R5	Backbiting 1,5 (1,4)	3.00×10^{8}	0	16,000
R5v	Backbiting 1,5 (1,2)	1.00×10^{9}	0	16,000
R6	Ene reaction	4.00×10^{10}	0	34,000
R7	Retro-ene reaction	9.00×10^{11}	0	48,000
R8	Intermolecular Diels-Alder	5.00×10^{9}	0	30,000
R9	Intramolecular Diels-Alder-like (isolated 1,2)	4.0×10^{13}	0	46,000
R10	Intramolecular cyclization (6-member ring)	1.00×10^{11}	0	21,000
R11	Intramolecular cyclization (5-member ring)	8.00×10^{11}	0	22,500
R12	Radical recombination	2.00×10^{11}	1	6,000

them into four allylic ones, with a consequent decrease in polymer reactivity. Conversely, the 1,2-crosslink loses four allylic positions but gains two diallylic structures, resulting in an overall increased reactivity compared to the starting vinyl units.

The reactivity of the two crosslinks involves both alkyl and allylic sites, as shown in Fig. 4. Among these, only the diallylic and allylic positions are assumed to contribute to the radical pool through initiation reactions (R1 and R1v, respectively), while H-abstractions from both alkyl and allylic hydrogens are considered. The former is unfavorable due to the lower stability of the resulting alkyl radical, but β-scission at these alkyl positions proceeds readily because it yields allyl radicals breaking the crosslink bond. Consequently, h-abstraction at alkyl hydrogens is assumed to be the rate-determining step responsible for de-crosslinking the structure, producing one stable and one radical MC unit, as shown in Fig. 5. In contrast, allylic hydrogens within the crosslinked unit are treated with a distinct species given their comparable stability to other hydrogens in the system. Nevertheless, the β-scission of these radicals is slower than that of other mid-chain ones, as it involves the formation of non-resonant radicals that then quickly decompose by β-scission into more stable allylic radicals. Since the first β-scission is significantly slower, the model lumps both steps in a single reaction, assuming the first step to be rate-limiting. The crosslinked allylic radicals may also form by decomposition of neighboring chains. Within functional group approach, this phenomenon is represented employing the crosslink species as SPU in unzipping and β-scission reactions. To simplify the model, these EC crosslinked radicals are represented by the MC ones, and result in formation of butadiene and the loss of the crosslinked structure. A more detailed representation of the crosslinked structure, introducing appropriate end-chains or multiple crosslinks species, could potentially enhance the model predictions of minor products such as cyclohexadiene and pentadiene. However, this refinement would considerably increase the number of species and reactions without sufficient experimental evidence to justify the added complexity.

The double bonds along the backbone allow for intramolecular radical additions starting from the terminal position. As shown in Fig. 6, the end-chain terminal radical can add on the unsaturated 1,4 microstructure through a six-member ring to form an alkyl radical that readily decomposes to release the cyclic dimer 4-vinylcyclohexene. The other product of this reaction is the reactant end-chain radical, yet with a polymeric chain eight carbons shorter. Fig. 6 depicts how this reaction is represented following the functional group approach. To represent the product polymer being shorter than the parent one, an additional SPU is consumed to regenerate the EC radical. This preserves the correct functional groups (a terminal HMW radical), while also representing the decrease in chain length [28]. The elementary steps of bond rotation, cyclization, and beta-scission are represented through a lumped reaction (R10) directly forming 4-vinylcyclohexene and P-C8H12_t, and the overall reaction is written in blue. The cyclic dimer is released as a gas, and the reactive end-chain remains in the condensed phase as a high molecular weight pseudo-species. The same reaction can take place also starting from the internal diene radical, releasing, however, 4-vinylcyclohexadiene. The model lumps all C_8H_{10} isomers, and therefore this reaction is represented by the beta-scission of the diene radical (P-C8H10_i) which generates the linear confomer.

The scientific literature reports, among the different degradation

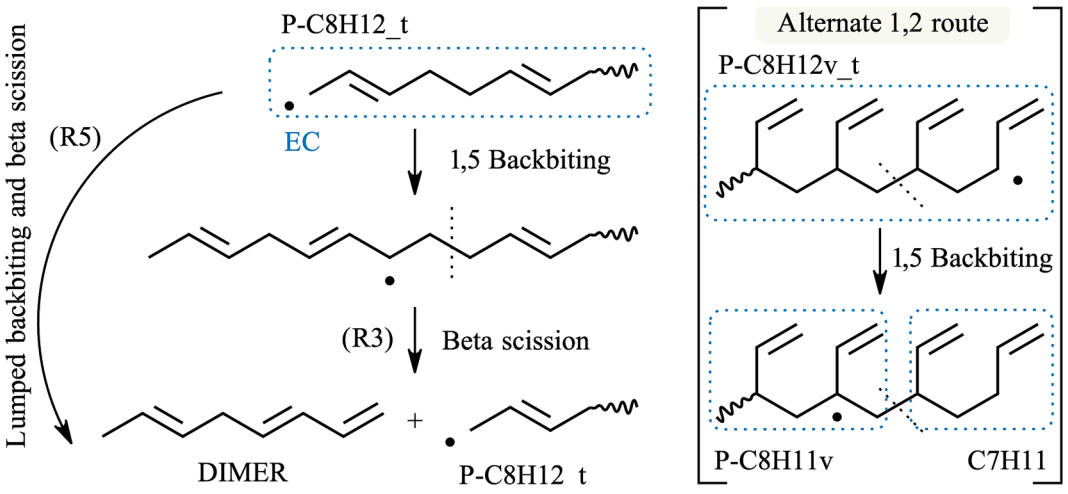

Fig. 3. Reaction mechanism for 1,5 backbiting of polybutadiene-derived end-chains to form dimers.

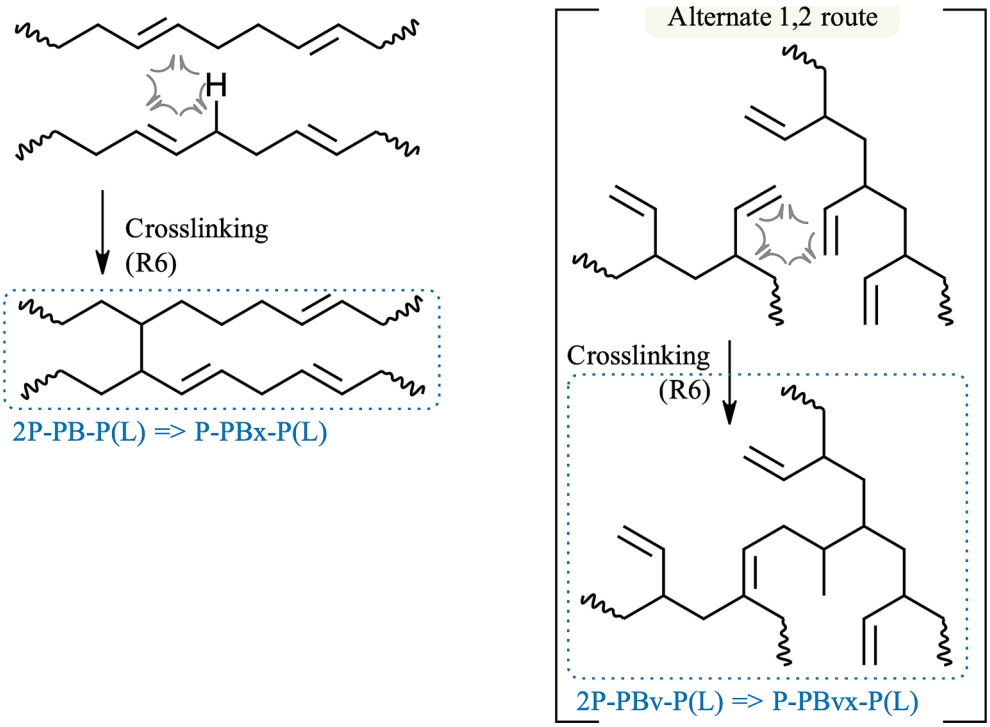

Fig. 4. Reaction mechanism for crosslinking of polybutadiene for both 1,4 and 1,2 moieties via ene reactions.

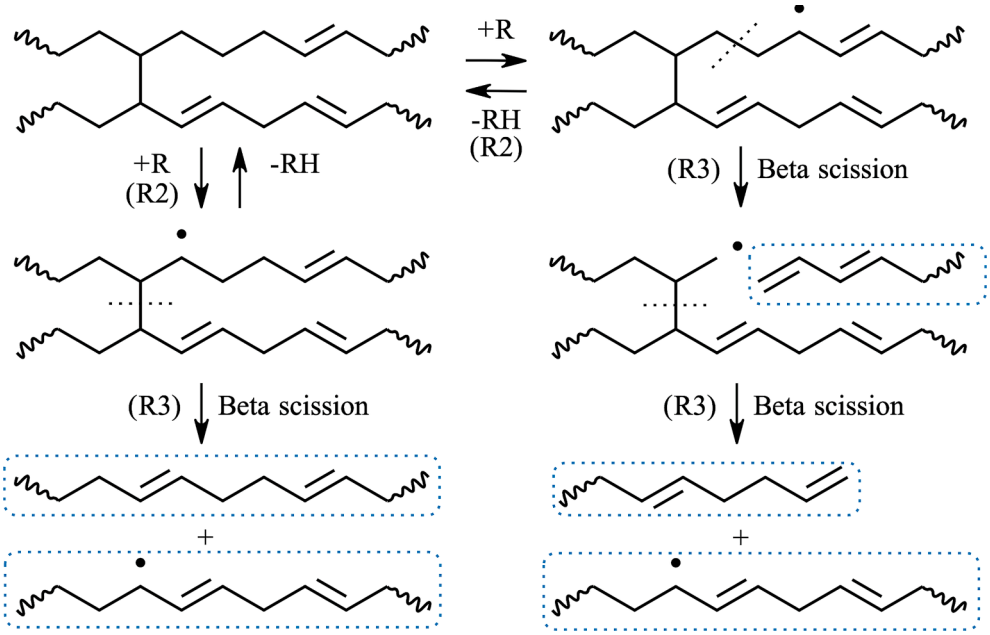

Fig. 5. Reaction mechanism for crosslink degradation via hydrogen abstraction and beta scission.

products, C_5 and C_7 compounds [13,30,40,43,69]. These compounds differ from the remaining volatiles as they are not oligomers but rather involve an odd number of carbon atoms. While C_7 products form as consequence of backbiting of 1,2 microstructures, the present model accounts for formation of these compounds through additional polybutadiene-specific reactions. A reaction that disrupts the even-numbered terminations is a retro-ene reaction involving a vinyl unit adjacent to a cis or trans site, as shown in Fig. 7. This reaction produces a terminal diene and a vinyl end-chain. While the vinyl end-chain invovled in this reaction is analogous to those formed through other reactions in the model, the diene, however, differs from the P-C8H11 1,4-microstructure diene shown in Fig. 2, as it features two carbon atoms, rather than one, separating the diene from the next double bond along the chain. The formation of the C_9 diene is among the reaction steps responsible for the formation of C_5 cyclic compounds. Intramolecular cyclization to form five-member rings from reactive end-chains is included in the model, as shown in Fig. 7. Following any h-abstraction at the hydrogen α to the diene, an internal cycloaddition through a five-member ring followed by β-scission forms cyclopentadiene and a terminal end-chain radical. Similarly, β-scission of the allylic radicals on the diene results in formation of a pentadienyl radical and a C_8 diene. In this work, to avoid introducing additional species, the

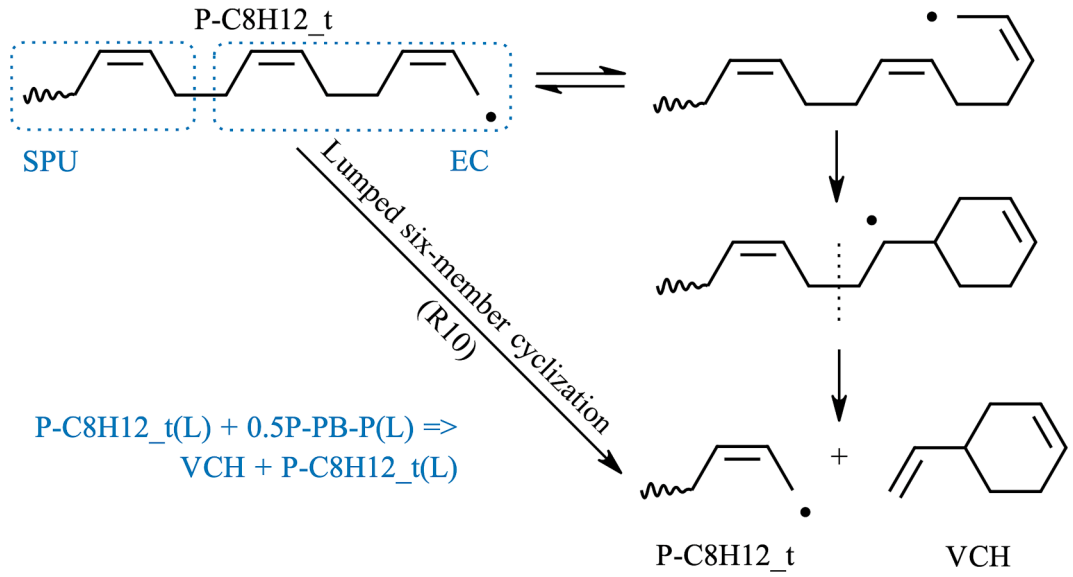

Fig. 6. Reaction mechanism for intramolecular cyclization of polybutadiene-derived end-chains to form 4-vinylcyclohexene.

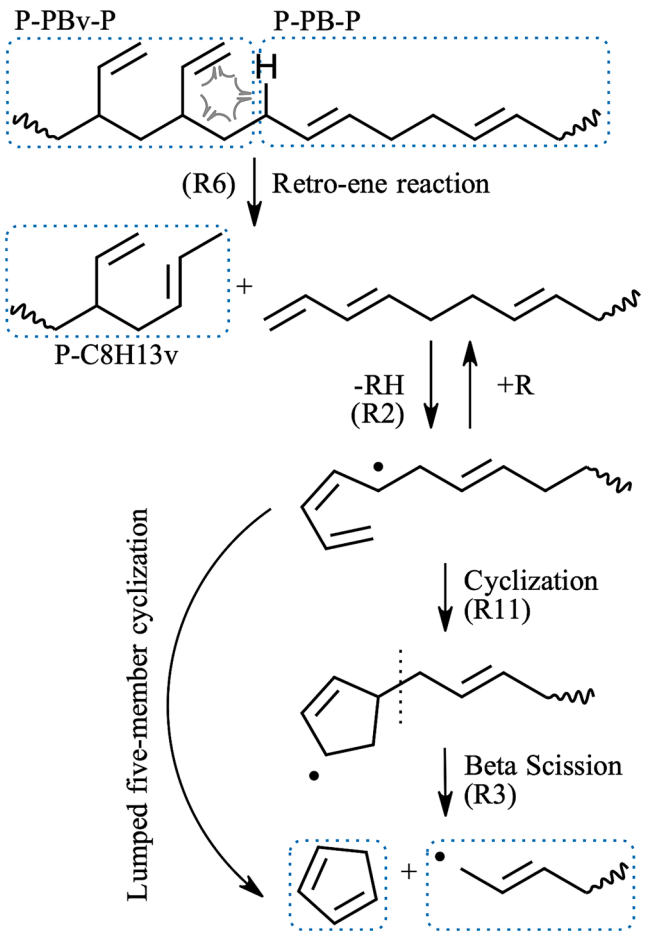

Fig. 7. Reaction mechanism for intramolecular retro-ene polybutadiene decomposition on a 1,2 microstructure neighboring a 1,4 microstructure and cyclization to form cyclopentadiene.

full sequence, including retro-ene reaction, end-chain cyclization and beta-scission, is lumped into a single reaction step, assuming the retro-ene is the rate-determining step. Remaining fragments are lumped into mid-chain and end-chain units, forming also C_2H_2 for the purposes of atom balancing with even carbon numbers. The reaction equation as implemented in the model is schematically represented in Fig. 7, where the model represents 1,4 and 1,2 neighboring units employing the vinyl microstructure as a SPU. The model considers five-member ring cyclization also on the P-C8H10_i end-chains. However, compared to the reaction shown in Fig. 7, it involves formation of a vinyl radical, which is significantly less stable than the allylic ones formed from the reaction shown in Fig. 2. Nevertheless, the reaction forming an allylic terminal radical can occur after double bond migration from the 6th to the 7th position, which may result from hydrogen abstractions on the 7th carbon and stabilization of the 6th carbon resonant position.

The model also considers bimolecular Diels-Alder reactions, depicted in Fig. 8, which represent another important class of reactions, albeit at a lower rate than free-radical pathways. These reactions involve diene end-chains forming six-member rings along the backbone. These rings detach following multiple allylic h-abstractions and β-scissions, breaking the bonds connecting them to the rest of the polymer. To avoid considering these numerous intermediate species, the model assumes the formation of the mid-chain ring structure to be the rate-determining step, modulating the reaction rate by the probability the ring will decompose back to the original reactants or will get released. Overall, the model considers one global reaction (R8) releasing 4-vinylcyclohexene and a toluene precursor.

A final reaction class incorporated in this model is the intramolecular cyclization of an isolated 1,2 moiety, forming 4-vinylcyclohexene via a Diels–Alder-like mechanism. This reaction (R9) occurs when a single vinyl moiety is flanked by cis and/or trans units, leading to ring closure and subsequent release of the six-membered cyclic product, as shown in Fig. 9. To the authors' knowledge, this reaction class has not been previously introduced in the context of PB pyrolysis, but a structurally similar reaction has been proposed in the catalytic depolymerization of PB at room temperature [70]. In that previous work, 1,4–1,2–1,4 triads (i.e., isolated vinyl units) were identified as chain limiters in metathesis reactions, with proposed ring-closing mechanisms yielding either cyclopentene derivatives or 4-vinylcyclohexene. Only the latter is incorporated because 4-vinylcyclohexene was a dominant species at low conversions, consistent with experimental observations of PB pyrolysis at moderate temperatures (<425 °C) [57]. The catalytic depolymerization study [70] proposed pathways similar to intramolecular cyclization using a structural basis that can occur thermally. Given the resemblance of this process to Diels-Alder mechanisms, the reaction rate parameters are adopted from a related intramolecular Diels–Alder reaction modeled

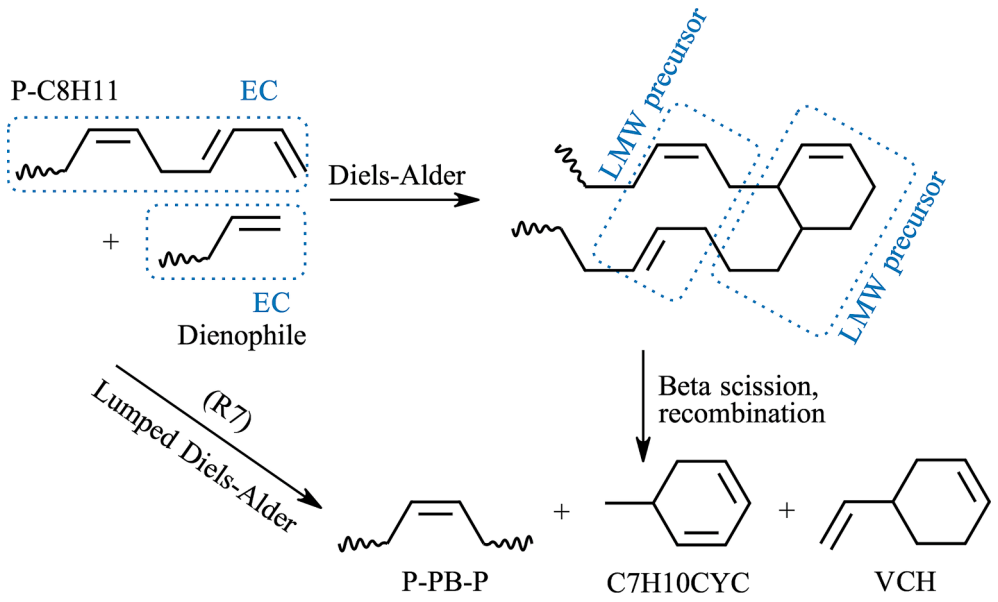

Fig. 8. Reaction mechanism for intermolecular Diels-Alder of a stable end-chain diene species and a stable end-chain dienophile species to form 4-vinylcyclohexene and toluene precursor.

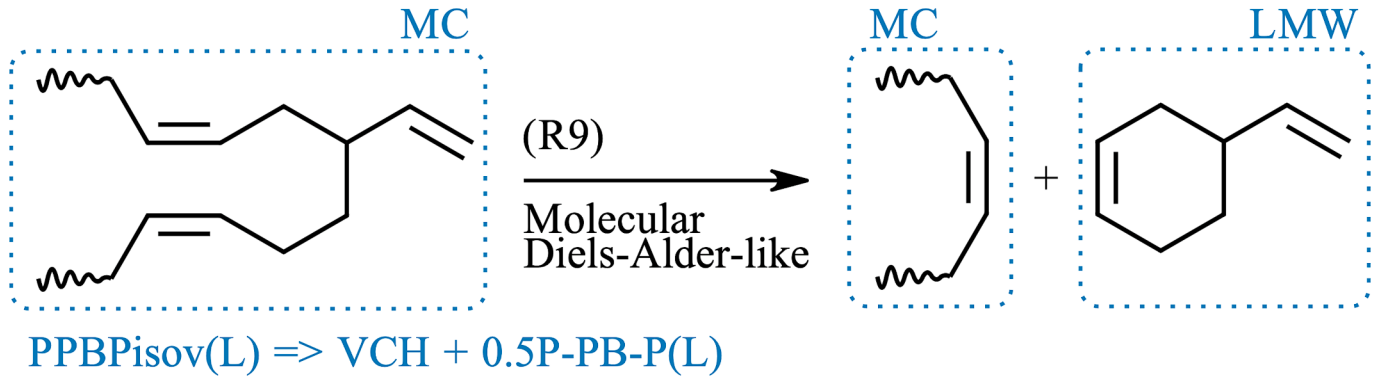

Fig. 9. Reaction mechanism for intramolecular Diels-Alder of an isolated vinyl moiety to form 4-vinylcyclohexene.

in polyvinyl chloride (PVC) decomposition [71].

The inclusion of this Diels–Alder-like reaction improves model accuracy for mass loss profiles and early-stage cyclic product formation, particularly in predicting the evolution of 4-vinylcyclohexene. Since vinyl content, and specifically isolated vinyl content approximated as described in section 2.2.1, directly influences its formation, this reaction class is essential for capturing the initial pyrolysis behavior of PB formulations with varying 1,2 and 1,4 microstructural composition.

2.2.4. *Kinetic parameters*

Accurate prediction of PB pyrolysis requires well-defined kinetic parameters for key reaction pathways. Table 2 presents a summary of key reaction types and their Arrhenius parameters, with reaction types distinguished between those for the cis or trans microstructure (e.g., R#) and those for the vinyl microstructure (e.g., R#v), if applicable.

The Arrhenius parameters for random scission reactions (R1) are based on analogous NIST data for 1,5-heaxdiene and 1,5-heptadiene [72], with a gas-to-liquid correction applied as described in previous work [28] and originally derived from a solvation correction applied to vinyl polymers [71]. Parameters to define the random scission of vinyl moieties (R1v) are derived from decomposition data for 3,4-dimethyl-1-pentene [73] and by analogy to polystyrene [66] and allyl radicals formation of small olefins [33], adjusted with the same gas-to-liquid correction.

Hydrogen abstraction reactions are evaluated for several scenarios, focusing on secondary and tertiary allylic carbons as the most reactive hydrogen donors for the 1,4 (R2) and 1,2 (R2v) microstructures respectively. For each reaction, rate parameters were assigned based on whether abstraction was performed by a primary, secondary, or tertiary carbon and according to the site abstracted. Per-site rate parameters specific to resonantly stabilized structures are employed [44]. The parameters for beta-scission reactions (R3, R3v) are derived using polyethylene (PE) [66] as a reference and following the corrections proposed by Mehl et al. [74]. For scission at 1,2 moieties, the activation energy is reduced by 1 kcal mol^{-1} compared to 1,4 moieties due to the formation of the more stable resonant structure. Unzipping (R4, R4v) rate parameters are derived analogously to PE [66] starting from the beta-scission, using a three times higher frequency factor and reducing the activation energy by 3 kcal mol^{-1} to reflect reduced caging effects [75]. Rate parameters for backbiting (R5, R5v) are defined similarly to polystyrene [66]. Specifically, the vinyl units have a higher frequency factor than in polystyrene due to the lower steric hindrance of the vinyl side groups compared to the aromatic rings. Conversely, a lower frequency factor is considered for the isomerization of the 1,4 microstructure, in line with the decrease in isomerization rate calculated by Wang et al. [76] for intramolecular additions.

For the polybutadiene-specific reactivity, the rate parameters are defined employing studies on analogous dienes and resonantly

stabilized radicals. The rate of ene reactions (R6) is obtained in analogy to the NIST database and the study of Popelier et al. [77], introducing a 2 kcal mol^{-1} decrease to account for the lower bond dissociation energy of secondary allylic hydrogens with respect to primary allylic ones. In this work, the same rate is considered for 1,2 and 1,4 unsaturation loss, as no clear trend is experimentally observed. For instance, Chiantore et al. [45] report 1,4 being as more reactive than 1,2, while Golub [46] reports the opposite trend. Nevertheless, the proposed rate parameters align with the experimental observations of Golub [46] for 1,4 unsaturation loss, and the ones of Chiantore et al. [45] for 1,2 unsaturation loss. The deviations may result from more complex reaction pathways that lead to unsaturation loss not considered in this work. The rate of retro-ene reactions (R7) is taken from the theoretical study of Popelier et al. [77], which accounts for the decrease in energy barrier for allylic hydrogens. Considering other molecular reactions, the same rates proposed by Marongiu et al. [78] for PVC are employed. Specifically, bimolecular Diels-Alder reactions involving six-member ring cyclization (R8) use the same rate parameters, reducing the rate was by a factor of 10 to account for the lower frequency of concerted addition reactions followed by beta-scission, rather than direct adduct formation. Similarly, the rate parameters of the four-member ring intramolecular cyclization (R9) are obtained starting from the study of Marongiu et al. [78], where the energy barrier is increased by 18 kcal mol^{-1} to account for the highly strained four-member ring in the transition state, and the frequency factor is increased by approximately $10^{1.6}$ due to the reduced number of hindered rotors involved.

Considering reactions involving resonant-stabilized radicals, the theoretical study of Wang et al. [76] is taken as reference. The rate parameters for the six-member intramolecular cyclization reaction (R10) are based on a reference endo-ring closure reaction [76] involving the same reactant as the C_8 end group of the modeled pseudo-species, with the primary distinction being that the end-chain in the model is longer due to the addition of the SPU (i.e., the attached polymer backbone). The reaction follows a 1,6-endo pathway, consistent with prior literature on free-radical cyclization in conjugated diene systems [76]. Given the near-identical structure, the same activation energy was initially applied, assuming the isomerization is the rate-determining step. The cyclization rate of five-member rings (R11) is obtained comparing 1,5-endo cyclization reactions described by Wang et al. [76] Compared to the 1,6 cyclization (R10), a higher frequency factor is considered to account for the reduced number of hindered rotors, and a 1.5 kcal mol^{-1} increase in activation energy to account for both the higher strain of the five-member ring and the higher stability of the radical intermediate. Finally, termination reactions (R12) are represented using diffusion-controlled rates [79] employing viscosity values reported by Van Krevelen [80].

3. Results and Discussion

3.1. Experimental data

3.1.1. Effect of heating rate on mass loss

The decomposition of polybutadiene in nitrogen at four heating rates is presented in Fig. 10, displaying thermogravimetric (TG) and differential thermogravimetric (DTG) profiles. The data in Fig. 10 are shown up to 600 °C for clarity, yet include, for all heating rates, that the DTG returns to zero, demonstrating the pyrolysis is complete. The experimental data are indicated by markers; simulation results, discussed in

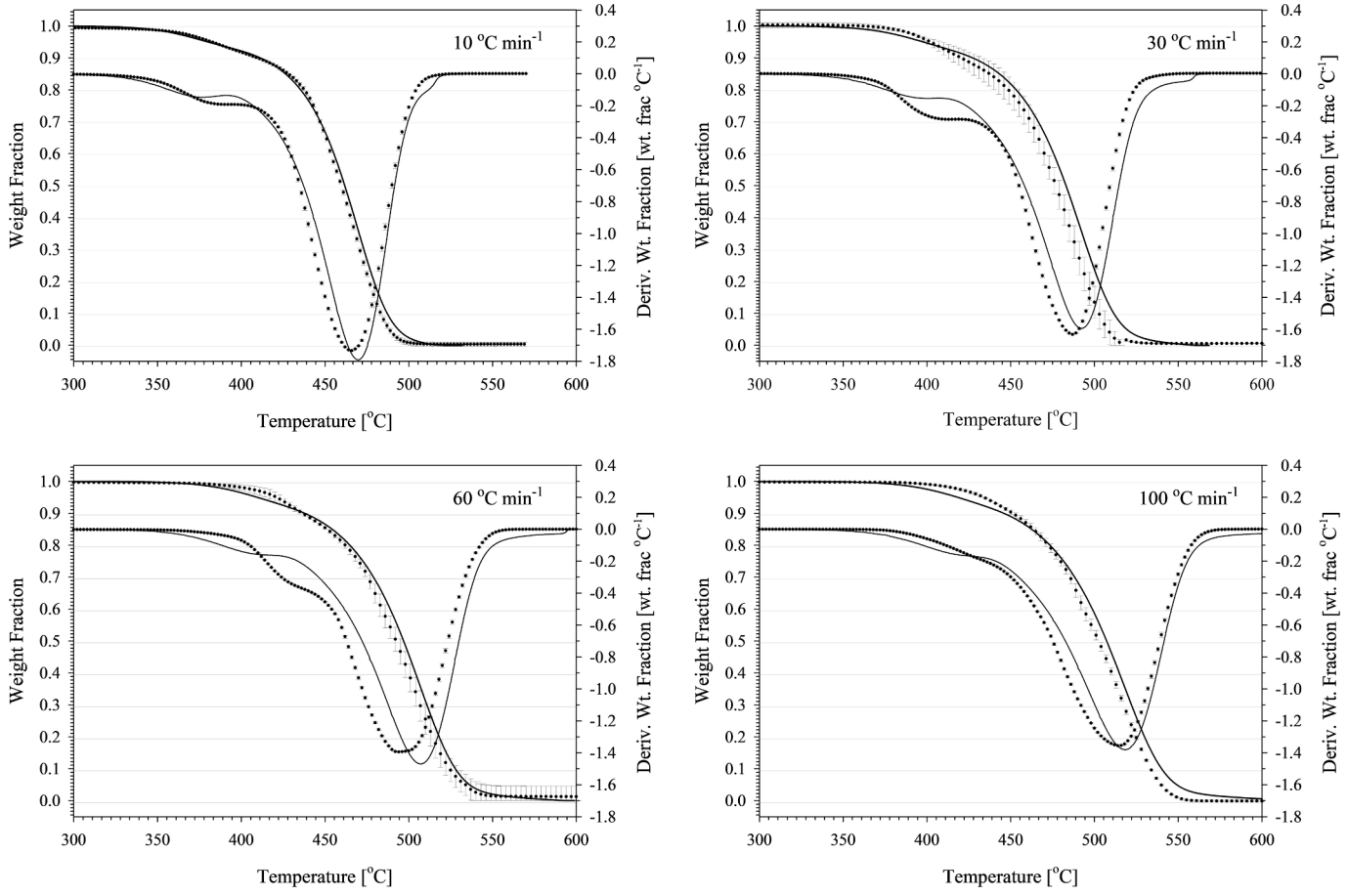

Fig. 10. Experiment TG and DTG curves (markers) of polybutadiene samples at a heating rate of 10 °C min^{-1}, 30 °C min^{-1}, 60 °C min^{-1}, and 100 °C min^{-1} compared to simulation TG and DTG results (lines).

section 3.2, are indicated by solid lines. The plotted data show the average weight fraction from triplicate experiments at each heating rate, with error bars indicating the standard deviation between individual measurements and the mean. Additionally, a representative DTG profile from one experiment, for clarity, with its simulation at the corresponding heating rate is plotted, showing the change in weight fraction as a function of change in temperature. The error bars on the DTG data account for the binning of high-frequency experimental data into discrete points spaced at 1 °C intervals. Across low to moderate heating rates, 10-100 °C min^{-1}, repeated experiments exhibit consistent mass loss trends. The DTG profile highlights two distinct decomposition events observed under all tested conditions.

Onset of the first mass loss event occurred at 348, 360, 358 and 369 °C for heating rates of 10, 30, 60, and 100 °C min^{-1} respectively, as determined from the second derivative of the mass loss versus temperature data. The onset of the second, dominant mass loss occurred at temperatures ranging from 470 °C for the 10 °C min^{-1} and 480 °C for the 100 °C min^{-1} heating rates. This decomposition regime extends until the remaining polybutadiene is completely volatilized. Importantly, final residues were zero, within the instrument's margin of error, demonstrating the purity of the polybutadiene sample. Finally, the DTG curves reveal the time–temperature shift of the peaks of the first decomposition event with the changing heating rates, from 377 °C at 10 °C min^{-1} to 441 °C at 100 °C min^{-1}.

Our data confirm two distinct stages of decomposition for pure PB at a heating rate up to 100 °C min^{-1}. Although reported literature presents inconsistencies, some previous studies corroborate this observation: experiments with commercial PB sourced from six manufacturers show two distinct stages of mass loss, including those with high cis (i.e., 95 wt %) PB at heating rates of 2 and 100 °C min^{-1} [54]. This has also been shown to be present for other microstructural compositions (77 wt% vinyl content and 55 wt% trans content) [54]. However, at 90 °C min^{-1}, vulcanized PB appears to suppress this two-stage behavior, though two stages remain evident at lower heating rates (15 – 45 °C min^{-1}) [30]. Notably, DTG results for the single-stage decomposition at heating rates above 45 °C min^{-1} show a broad primary decomposition peak flanked by two smaller peaks, revealing overlapping decomposition events. These observations align with studies showing that butadiene rubber exhibits two distinct decomposition stages even at heating rates as high as 80 °C min^{-1} [18,60]. Discrepancies in reported decomposition stages may stem from polymer microstructure, contaminants, or misinterpretation of TGA data, particularly when DTG is not reported. For example, it has been demonstrated that high vinyl content PB at 10 °C min^{-1} exhibits a single-stage decomposition by TGA, but DSC data reveal exothermic and endothermic events, indicating overlapping chemical processes [67]. Similar complexities arise at intermediate heating rates, where TGA alone suggests a single stage, yet DTG and DSC analysis highlight two distinct chemical regimes [67], emphasizing the necessity of multi-technique analysis for accurate characterization. The kinetic mechanism proposed in this work provides further insight into the first decomposition stage, offering a framework to reconcile discrepancies in the literature and predict conditions under which two stages of decomposition are likely to occur.

3.1.2. *Validation of experimental data against literature*

Our experimental mass loss profiles resulting from PB pyrolysis are validated against literature data [18,31,55,58,68,81] to ensure accuracy and fidelity. Given the variability in reported mass loss profiles under similar conditions, careful benchmarking was performed against both analogous polymers (e.g., hydroxyl-terminated polybutadiene [58,68,81]) in Fig. 11 and direct PB [18,30,31] literature data in Fig. 12, Fig. 13, and Fig. 14), with key test parameters summarized in Supplemental Materials Table S1.

As shown in Fig. 11, the PB degradation experiments reported in this work at 10 °C min^{-1} are compared to relevant literature studies conducted at the same heating rate albeit with differences in sample

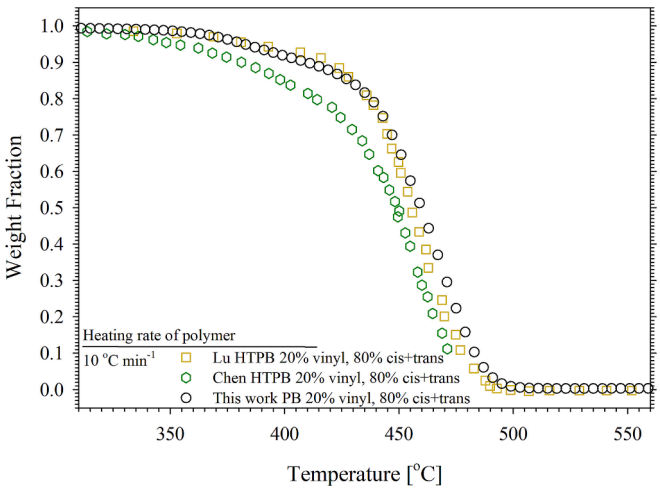

Fig. 11. TG curves of hydroxyl-terminated polybutadiene samples from existing literature results compared to new uncured polybutadiene data [this work] at heating rates of 10 °C min^{-1}.

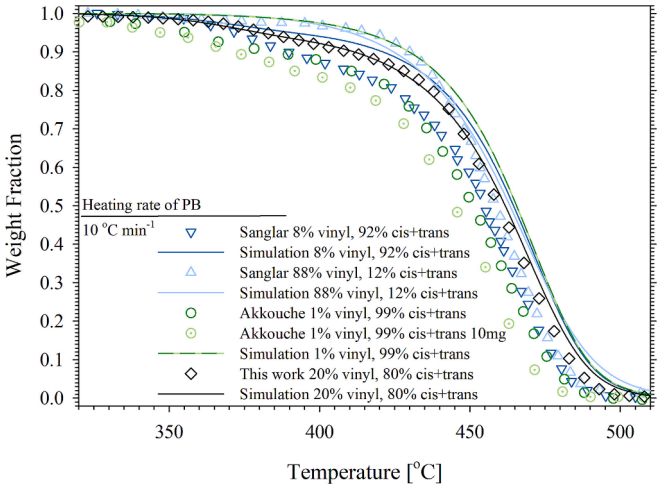

Fig. 12. Simulated TG curves (lines) compared to experimental data (markers) of polybutadiene samples at heating rates of 10 °C min^{-1}.

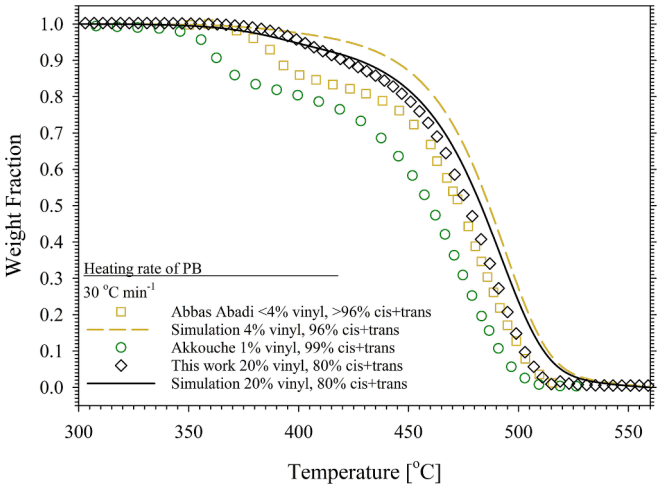

Fig. 13. Simulated TG curves (lines) compared to experimental data (markers) of polybutadiene samples at heating rates of 30 °C min^{-1}.

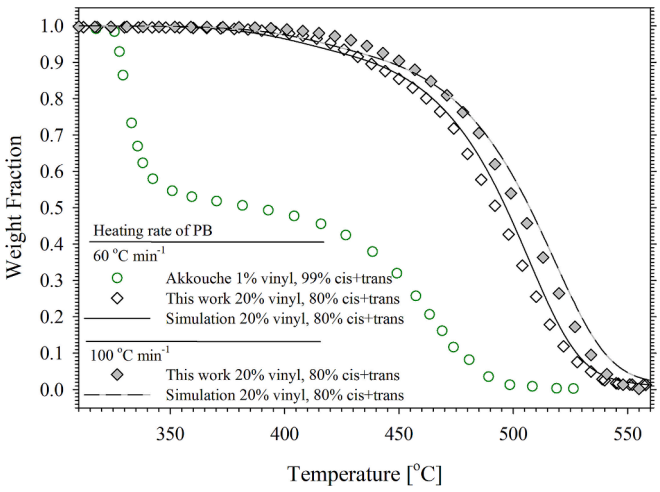

Fig. 14. Simulated TG curves (lines) compared to experimental data (markers) of polybutadiene samples at heating rates of 60 °C min^{-1} and 100 °C and 100 °C min^{-1}.

characteristics, such as cis, trans, vinyl ratios and TGA configurations. HTPB studies from Lu & Kuo [58] and Chen & Brill [68] show minor discrepancies, particularly at early conversion, likely due to differences in sweep gas (N_2 vs. Ar), TGA configuration (vertical vs. horizontal purge gas flow), and preheating conditions. However, by 60 % conversion, these datasets converge.

Fig. 12 compares model results with mass loss profiles of various pure PB samples at 10 °C min^{-1}. The model was employed to simulate both the new data presented in this work and the preexisting literature data. The data show both faster and slower decompositions compared to this work, with only the work of Akkouche et al. revealing a smaller initial decomposition step followed by a larger one, which is consistent with the findings of the present work. The current results demonstrate the expected trend of higher heating rates causing decomposition temperatures to shift upward. The results here reported are typical compared to the majority of observed trends in the literature for decomposition of PB [55,67], HTPB [58,81–84], polybutadiene rubber [62,85], natural rubber [85], polybutadiene-co-acrylonitrile [81], and styrene-butadiene rubber [85]. However, not all literature data align with the new experimental results at higher heating rates reported in this work. As shown in Fig. 13, at 30 °C min^{-1}, and more acutely in Fig. 14 at 60 °C min^{-1}, Akkouche et al. report an opposite trend as compared to lower heating rates—where increasing heating rates advance mass loss onset rather than delay it, which the current data do not replicate. Up to 100 °C min^{-1}, the results of the present work consistently show mass loss shifting to higher temperatures with increasing heating rates, as expected.

Akkouche et al. attribute their trend reversal to self-heating effects, where endothermic and exothermic reactions alter the sample temperature independently of the furnace. Their study showed that for large PB samples (≥30 mg), thermal gradients were significant, leading to self-heating effects that advanced the mass loss profile. Self-heating increased sample temperatures by up to 25 °C above the furnace set-point, affecting decomposition behavior. They found that reducing the sample size to 10 mg minimized these thermal effects, ensuring accurate TGA measurements. This effect has also been reported for large samples of biomass [86]. Abbas-Abadi et al. reported a similar trend reversal behavior to Akkouche et al.: as heating rates increase from 30 to 45 to 90 °C min^{-1}, degradation temperatures advance. Abbas-Abadi et al. used a 12 mg sample, which is close to the 10 mg threshold recommended by Akkouche et al. However, it is suggested that sample mass suitability depends on crucible design [87]—Akkouche's experiments used a 130 μL cylindrical crucible with a low height-to-diameter ratio (~25 %), whereas Abbas-Abadi did not specify their crucible type. In this study, a similarly sized crucibles (100 μL) and sample masses between 5.7–11.0 mg are employed, ensuring shallow pan conditions comparable to Akkouche et al. The data reported in this work exhibit no evidence of self-heating effects up to 100 °C min^{-1}. Consequently, they are not expected to match the 60 °C min^{-1} data from Abbas-Abadi et al. Only in two other studies did the trend reversal, as seen in Abbas-Abadi et al. and Akkouche et al., occur, though only at high heating rates of 75 and 100 °C min^{-1}, and only for some types of samples (high cis PB [67], random crosslinked PB [67], and crosslinked HTPB [58]).

3.2. Simulation

3.2.1. Validation of model-derived mass loss profiles with experimental data

The modeled mass loss profiles of PB as a function of temperature compared against both literature data and experimental results from this study are presented in Fig. 12, Fig. 13, and Fig. 14. In those figures, each relevant experimental dataset is paired with a corresponding simulation conducted under matching conditions. Since the model does not differentiate between cis and trans microstructures, it provides a single prediction value for all PB samples of a given vinyl content. For instance, to model the Sanglar et al. experiment with pyrolyzed PB (33 wt% cis, 59 wt% trans, 8 wt% vinyl) at 10 °C min^{-1} [31], a simulation was performed using PB with 92 wt% 1,4 and 8 wt% 1,2 microstructures at the same heating rate. Akkouche et al. conducted experiments with 30 mg and 10 mg samples [18], both shown in Fig. 12, but a single simulation at 1 wt% vinyl was used for comparison. Additionally, the model is used to simulate the new experimental data, providing further validation of its predictive capability.

Mass loss profiles at heating rates of 10, 30, 60, and 100 °C min^{-1} demonstrate the model's performance in predicting key decomposition behaviors. The model effectively reproduces the region of maximum mass loss rates while capturing the initial and final stages of decomposition. Moreover, the model accurately predicts the complete conversion of PB to gaseous products with no residual mass remaining. The average discrepancy between the simulations and the data ranges from 0 wt% to 6 wt% at a given temperature, resulting in a 2 wt% overall average. This discrepancy falls within the range of discrepancies among experimental data [18,30] as reported in the literature.

According to the simulation, the first decomposition peak, yielding a 5 wt% mass loss, is due to intramolecular cyclization via molecular Diels-Alder-like reactions of the isolated 1,2 microstructures (R9) that contribute to 56 % of the 5 % mass lost. At the same conversion, the next most predominant reactions are hydrogen abstraction (R2) to form high molecular weight reactive species and unzipping of 1,4 moieties (R4) to form the monomer. Deviations between the model and experimental results during the initial stage of mass loss are observed. Early-stage cis–trans isomerization reactions [55,88] are known to retard the onset of mass loss by up to 50 degrees [31]. Their omission from the current model contributes to the deviations between the model and experimental results in this region, yet the model is still able to capture the early-stage decomposition exhibited by feedstocks containing vinyl moieties due to the inclusion of the novel isolated-vinyl Diels-Alder-like molecular reactions.

Molecular Diels–Alder reactions involving isolated 1,2 moieties become negligible, according to the model, after the initial decomposition event (i.e., at mass loss greater than 10 wt%), with product formation rates a result of these reactions only reaching $-5.25\text{x}10^{-7}$ kmol m^{-3} s^{-1} due to their prior consumption. Although hydrogen abstraction reactions are still prevalent at this extent of reaction, competing random scission (R1) and unzipping reactions gain significance at these higher temperatures. Between 10 % conversion and 25 % conversion, product formation rates due to hydrogen abstraction reactions only increase by a factor of 2.6, whereas those due to unzipping reactions increase by a factor of 14.8. Random scission increases by a factor of 1.3. Finally, after

an initial rate of production peak of 60 % from 0-5 % conversion, cyclization to form six-carbon compounds from 1,4 moieties (R12) provides a nominally consistent contribution for decomposition (8.9–11.7 %) at all heating rates throughout intermediate extent of reaction until 90 % conversion, with the other product species, predominantly butadiene, comprising the balance of produced species.

The advanced stages of decomposition (i.e., 90 wt% conversion), reveal that random scission becomes more dominant, overtaking some hydrogen abstraction reactions in terms of rate of consumption of the parent polymer. Unzipping, which is an important component throughout the decomposition process, continues to contribute significantly from 50 wt% loss to 90 wt% loss, aligning with the high production of butadiene. Likewise, 4-vinylcyclohexene formation is consistently prominent. Secondary reactions produce precursors to these major products or aliphatic oligomers, as observed in short-lived intermediates in other work [63].

A reaction rate sensitivity analysis, provided in Supplemental Materials Fig. S2, demonstrates that mass loss profiles are generally robust to parameter variations. Maximum deviations from baseline were limited to 15 °C under a twofold increase or decrease in reaction rates. However, the model is most sensitive to the random scission of 1,4 microstructures, influencing mass loss across the entire decomposition sequence. Random scission is the only reaction class to significantly impact the temperature at which complete volatilization occurs. As a sensitivity parameter, hydrogen abstraction follows in importance, with its impact more pronounced at lower heating rates.

3.2.2. *Product speciation*

Model validation was performed by simulating results under the same microstructure and heating rate conditions as those reported in previously published experimental datasets, focusing on speciation during bulk mass loss [30,69] and early-stage (15 wt% conversion) [40]. Additionally, flash pyrolysis datasets from the literature [30,69], relevant to propulsion applications, were used for benchmarking. A comparison of the simulation result to literature experimental data for overall product speciation is reported in Fig. 15 (slow pyrolysis, Choi [69]) and in the Supplemental Materials Table S2 (rapid pyrolysis, Abbas-Abadi et al. [30]) for PB samples containing 3 %, 24 %, 26 % or 69 %, and $\leq$ 2 % vinyl microstructures respectively. The model has been validated on condensed phase reactions and is the only detailed mechanism for PB thermal decomposition. Therefore, samples with very different microstructures or additives may require possible adjustments to the major reaction rates to incorporate those effects.

The literature-reported speciation from the entire decomposition process is uneven in degree of uncertainty, as the identified and quantified gaseous compounds account for only 53–70 wt% [69] of the total products formed. The balance fraction of unreported gases in the literature may be due to deposition of condensed species at high heating rates [30], or due to the presence of up to 70 low abundance volatile species detected in the study [43] which are not all identified and quantified. The butadiene monomer constitutes a significant fraction of the products from the literature studies, with values ranging from 39 to 46 wt%. Abundance of C_5-C_9 species, including 4-vinylcyclohexene, varies significantly from 15 to 24 wt%, with large contributions from C_8H_{12} particularly at higher values (17 and 19 wt%). Lower fractions of C_8H_{12} (8 wt%) correspond to the lowest total reported mass fraction (53 wt%). This leaves a large portion of species unreported in the literature, creating uncertainty about the speciation, including large molecules with 10 or more carbon atoms.

The model is in close agreement, within 7.06 wt% absolute on average, with the experimental speciation data from the literature. It satisfactorily predicts the 4-vinylcyclohexene, the oligomer, and the combined cyclopentene and cyclopentane species production, with reasonable accuracy within 15 wt% for both the low vinyl (3 %) and moderate vinyl (25 %) content PB. Yet, at higher vinyl (69 %) content, the model over predicts the combined five-carbon to nine-carbon species by a factor of 7.72 in the worst case. Butadiene predictions are very close to the literature data, within 4.04 wt% absolute at maximum deviation, with an average difference of 2.13 wt%.

In addition to speciation during bulk mass loss, speciation data at low conversion provides valuable insights into the early stages of decomposition. Accordingly, Fig. 16 reports the model simulated product

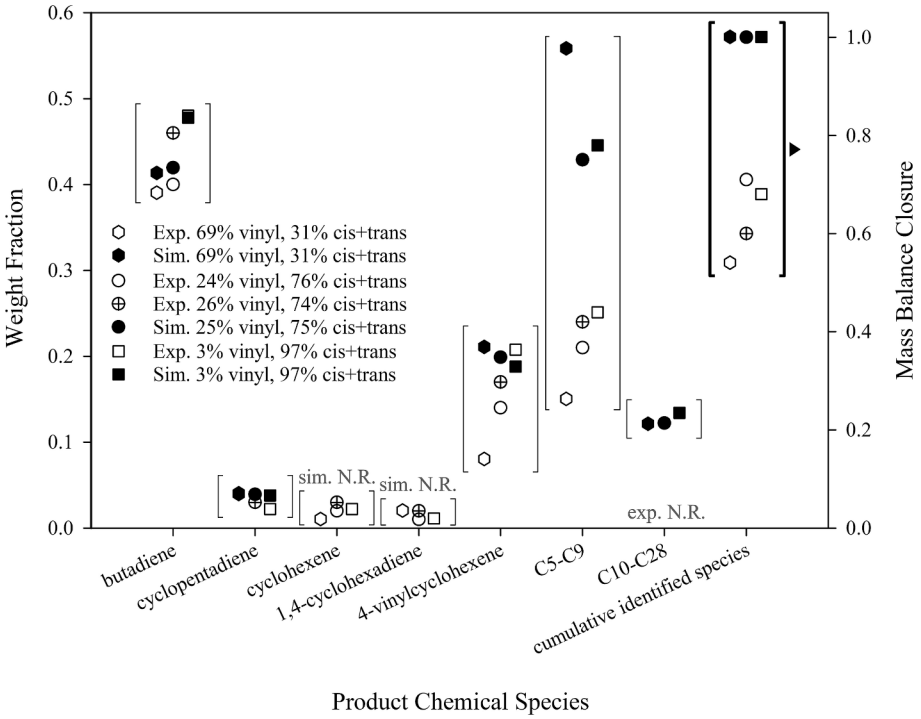

Fig. 15. Comparison of product species (by weight) from slow pyrolysis of polybutadiene at 8 °C min^{-1} at 590 °C for feedstocks of varying microstructural composition.

distribution at early-stage decomposition stages for PB samples each containing 1 % vinyl microstructures. Literature data [40] of eight formulations with nominally zero vinyl content but varying cis:trans ratios were used for validation. All samples were pyrolyzed at a heating rate of 20 °C min^{-1}.

The experimental data in Fig. 16 indicate that butadiene and 4-vinylcyclohexene are among the most abundant species at 15 % mass loss. This is consistent with simulation results, which show that the P-C8H12_t species undergoes rapid unzipping leading to the formation of butadiene and regeneration of the same end-chain species.

The model correctly predicts the production of the two major species, namely butadiene and 4-vinylcyclohexene at 15 % mass loss. The omission of 1,3 cyclohexadiene from the model is justified by its low abundance (≤ 5 wt%) at 15 % mass loss and its absence as a significant product at later conversions, as indicated by the experimental data [30,69]. However, the model underestimates the combined formation of cyclopentene and cyclopentane formation by up to 5.7 wt% absolute for formulations with less than 80 % trans content, and by up to 12.3 wt% absolute for high-trans formulations. This is due to the exclusion of reaction pathways in the model that are known to form cyclic species such as via a three-member ring to five-member ring route [89] and during crosslinking [90]. For other species, agreement between the model and the experimental data is closest for the formulations with trans content lower than 86 %. Despite predicting 4-vinylcyclohexene within the 24.1 wt% of the literature experimental range, the model overestimates butadiene in all cases, but with the largest discrepancy (by 32.0 wt% absolute) as compared to a case with high trans content (86 % trans). When only considering the agreement between the model and the experimental data pertaining to PB samples with trans content lower than 86 %, production of 4-vinylcyclohexene and butadiene are estimated well, within a factor of 1.6, and only the cyclopentene production is more significantly underestimated, by a factor of 7.9, on average.

To test the applicability of the model, comparisons were conducted for a flash pyrolysis experiment from the literature [30]. The experimental speciation data only accounted for the condensed liquid fraction, omitting C_4 species that remained in the gas phase. Therefore, the butadiene formation is underestimated, thus explaining the model's higher predicted yield. These results can be found in Table S2 of the Supplemental Materials.

Finally, the model was validated against the product speciation obtained in this study by py-GC/MS analysis of the evolved gases. Table 3 reports the species measured in excess of 2 wt% across four temperatures during the pyrolysis of PB at a heating rate of 2 °C min^{-1}. By this method, a temperature resolved speciation was captured across the decomposition profile, from low conversion to high conversion, including a period of high rate of mass loss, at 4.2, 7.3, 30.8, and 84.8 wt % conversion respectively. The results indicate the production of gaseous species at the discrete measurement temperature, rather than a cumulative result up until the measurement temperature. Butadiene monomer was found to be the species with highest mass rate of production at both 350 and 375 °C, at 32.2 and 58.1 wt% respectively. At the first of two stages of mass loss, 4-vinylcyclohexene was detected, comprising 5.5 wt% at 350 °C, supporting the formation mechanism proposed in the model. At higher temperatures, butadiene production decreases in favor of formation of larger compounds, including those with greater than 10 carbon atoms. As compared to the model, both butadiene and 4-vinylcyclohexene rates of production at 420 and 450 °C are lower than expected. It is possible that those compounds are participating in secondary reactions at those elevated temperatures and at those elevated concentrations in the effluent gas stream due to a higher rate of mass loss than at the lower temperatures. The experimental measurement of product species confirmed the production of predominant gaseous species included in the model, and revealed the presence of several species not previously measured in the literature as products of pure PB pyrolysis. The measurement of toluene in the evolved pyrolysis gases is supported by the model prediction of C7H10CYC, a toluene precursor. Toluene has not been directly measured as a product of pure polybutadiene pyrolysis in other studies [17,30,40,67,69,91]. In this work, 34 gaseous species were identified and quantified. A comprehensive comparison of all identified species in this work and in the literature can be found in Supplemental Materials Table S3.

Table 3
Measured products of pure PB pyrolysis at various temperatures heated at 2 °C min^{-1}.

Carbon number	Species	Mass fraction of species over 2.0 wt% [wt%] Temperature [°C] 350	375	420	450
C4	Butadiene C4H6	32.2	58.1	8.7	7.6
C5		2.7	6.2	5.0	2.8
	1,3-Cyclopentadiene C5H6		6.2	0.8	
	Cyclopentene C5H8	2.7		1.2	1.2
	1-Pentene C5H10			2.9	1.6
C6		17.8	18.0	21.3	2.1
	Benzene C6H6	4.2	14.5	1.4	
	Cyclohexadiene C6H8	2.5	3.5	2.6	1.1
	Cyclohexene C6H10	11.1		0.4	
	1,4-Pentadiene, 2-methyl- C6H10			14.0	
C7		16.5	17.7	48.0	2.1
	Toluene C7H8	16.5	17.7	5.6	
	1,4-Cyclohexadiene, 1-methyl- C7H10			2.8	
	C7H10			13.1	2.1
	C7H12			22.9	
C8		30.7		4.8	3.2
	C8H10	2.4			3.2
	4-vinylcyclohexene C8H12	5.5			
	Cyclopentadiene, 2,5,5-trimethyl- C8H12	5.6			
	Cyclopentene, 1,2,3-trimethyl- C8H14			3.3	
	C8H16	17.2			
C10+					77.4

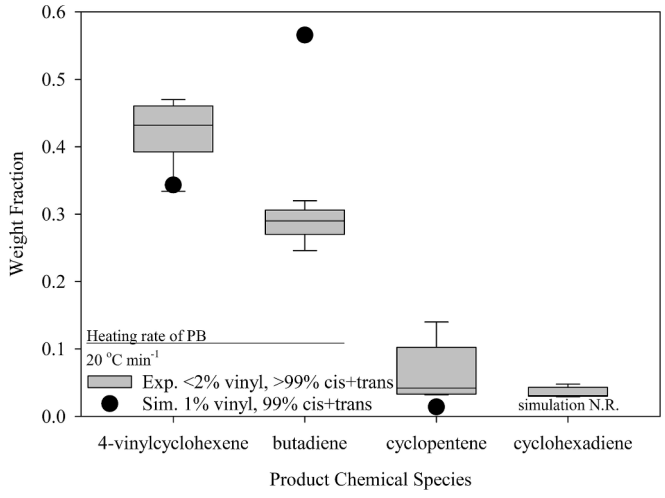

Fig. 16. Relative abundance of product species (by weight) from pyrolysis of polybutadiene at 20 °C min^{-1} at 15 % mass loss with simulated results compared to experimental results from the literature.

3.2.3. *Effect of vinyl content on mass loss profile*

Modeling the early-stage (i.e., temperatures from 325 to 425 °C) pyrolysis of PB presents significant challenges due to simultaneous reactions that precede the onset of volatilization [67] such as isomerization and crosslinking. While the model does not explicitly include the isomerization reactions, it does capture crosslinking and cyclization

reactions associated with low-temperature degradation, particularly those originating from the 1,2 moiety reaction pathway. One key reaction incorporated in this study is the intermolecular Diels-Alder-like reaction of isolated 1,2 units, introduced here for the first time as a major contributor to low-temperature degradation.

To assess the accuracy of the model in capturing early-stage vinyl-dependent mass loss behavior, simulations were performed using two distinct PB feedstocks: one with 88 % initial vinyl content and another with 8 %, matching available literature data. Fig. 17 compares experimental DTG data from Sanglar et al. [31] with corresponding model predictions. The experimental data at 10 °C min^{-1} reveal a distinct mass loss peak between 350 and 400 °C in the low-vinyl sample (8 wt%), which is notably absent in the high-vinyl sample (88 wt%). The proposed model successfully replicates this trend, demonstrating that it appropriately accounts for vinyl-dependent degradation pathways. Furthermore, both the temperature at which the maximum rate of mass loss occurs and the magnitude of the peak decomposition rate are well captured for both compositions. These results validate the model's ability to describe the influence of vinyl content on PB decomposition and reinforce the importance of including vinyl-specific reaction pathways in predictive kinetic frameworks.

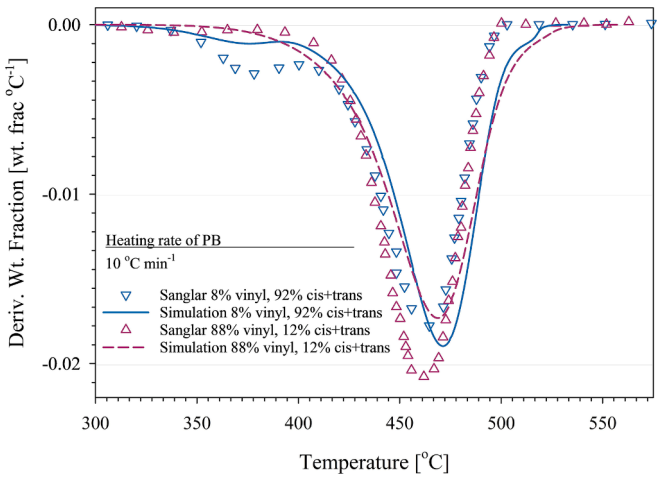

Fig. 17. Simulated DTG curves (lines) of polybutadiene samples at 10 °C min^{-1} compared to experimental data (markers) and high and low vinyl content PB.

4. Conclusions

This study investigates the thermal degradation of polybutadiene, introducing the first semi-detailed chemical kinetic model capable of describing decomposition pathways of the polymer that are relevant to the subsequent combustion of product gases. This work provides additional experimental targets to drive kinetic model development. The objectives are to elucidate the behavior of polybutadiene in pyrolytic environments and to develop predictive kinetic models describing the polymer mass loss and the release of volatiles. Experimental investigations utilized thermogravimetric analysis for quantitative analysis.

The findings highlight the model's ability to capture key pyrolysis mechanisms. Such modeling is crucial for interpreting experimental results characterized by proposed reaction classes and predicting combustion characteristics of produced gases that are then ignited in the gas-phase in targeted applications. This integrative approach leverages experimental and modeling techniques to provide a mechanistic understanding of polybutadiene pyrolysis under various heating rates, thereby enhancing the predictive capabilities in practical applications.

Summarizing

- This study introduces the first chemical kinetic model that predicts species formation during the condensed-phase pyrolysis of polybutadiene, providing a foundational understanding of its decomposition behavior.
- New thermogravimetric analysis data offer highly relevant benchmarks for refining pyrolysis models, ensuring accurate representation of decomposition mechanisms especially at high heating rates where thermal effects can dominate kinetic effects.
- This model highlights the importance of incorporating additional reaction pathways, such as the novel intramolecular Diels-Alder-like reactions involving isolated vinyl moieties, to enhance predictive accuracy in early-stage decomposition and lower heating rates.
- This work measures and predicts evolved gaseous chemical species from pyrolysis of PB that can be used to inform how those gaseous species would perform when combusted for relevant applications such as propulsion and energetic materials.

CRediT authorship contribution statement

Lauren T. Creadore: Writing – original draft, Visualization, Software, Methodology, Formal analysis, Conceptualization. **Andrea Locaspi:** Writing – review & editing, Software, Methodology, Conceptualization. **Tricia M. Marchese:** Investigation. **Matteo Pelucchi:** Writing – review & editing, Supervision, Conceptualization. **Tiziano Faravelli:** Writing – review & editing, Supervision, Project administration, Conceptualization. **Marco J. Castaldi:** Writing – review & editing, Visualization, Supervision, Project administration, Formal analysis, Conceptualization.

Declaration of competing interest

The authors declare that they have no known competing financial interests or personal relationships that could have appeared to influence the work reported in this paper.

Acknowledgements

The Earth Engineering Center at The City College of New York is greatly appreciated for providing the funding for this work.

Appendix A. Supplementary data

Supplementary data to this article can be found online at https://doi.org/10.1016/j.fuel.2025.136572.

Data availability

Data will be made available on request.

References

[1] U.S. Tire Manufacturers Association, 2023 End-of-Life Tire Management Report. U. S. Tire Manufacturers Association; 2024. [Online]. Available: USTires.org, "2023 ELT Tire Report Page".
[2] Rahman MM, Yu Y, Wu H. *Valorisation of Waste Tyre via Pyrolysis: advances and Perspectives*. Energy Fuel 2022;36(20):12429–74.
[3] Barford A, Ahmad SR. *Levers for a corporate transition to a plastics circular economy*. Bus Strateg Environ 2023;32(4):1203–17.
[4] Coleman, B., et al., *LCA carbon footprint summary report for Eastman carbon renewal technology*. 2020, Eastman Chemical Company.
[5] Russ, M., M. Gonzalez, and M. Horlacher, *Evaluation of Pyrolysis with LCA – 3 Case Studies* 2020, Sphera Solutions GmbH.
[6] Zhang Q, et al. *Hydroxyl terminated polybutadiene: Chemical modification and application of these modifiers in propellants and explosives*. Cent Eur J Energetic Mater 2019;16(2):153–83.
[7] Gromov A, Zarko V. Energetic Nanomaterials: Synthesis, Characterization, and Application 2016.
[8] Hedman TD. *Radiation-induced pyrolysis of solid fuels for ramjet application*. Propul Power Res 2016;5(2):87–96.
[9] Hedman TD, et al. *Small-Scale Solid Ramjet fuel Ignition Experiment*. J Propul Power 2017;33(5):1315–9.

[10] Chapman WW, et al. *Shock-induced reactions in metal nitride – Boron nanostructured composites*. Scr Mater 2020;189:58–62.
[11] Jung K, Cho M, Zhou M. *Thermal conductivity prediction for GaN nanowires from atomistic potential*. AIP Adv 2013;3(7):072123.
[12] McQuaid M, Chen C-C, Stone C, Jeffrey DV. *On Modeling the Pyrolysis of Hydroxyl-Terminated Polybutadiene (HTPB). Type R45M at Temperatures in the Range 465-600 °C*. 2023.
[13] Choi S-S, Han D-H. *Pyrolysis paths of polybutadiene depending on pyrolysis temperature*. Macromol Res 2006;14(3):354–8.
[14] Lah B, Klinar D, Likozar B. *Pyrolysis of natural, butadiene, styrene–butadiene rubber and tyre components: Modelling kinetics and transport phenomena at different heating rates and formulations*. Chem Eng Sci 2013;87:1–13.
[15] Menares T, et al. *Waste tires pyrolysis kinetics and reaction mechanisms explained by TGA and Py-GC/MS under kinetically-controlled regime*. Waste Manag 2020;102:21–9.
[16] Ranzi E, et al. *Reduced Kinetic Schemes of complex Reaction Systems: Fossil and Biomass-Derived Transportation Fuels*. Int J Chem Kinet 2014;46(9):512–42.
[17] Saha T, Bhowmick AK. *High-temperature degradation of butadiene-based model elastomers by reactive molecular dynamics simulation*. J Appl Polym Sci 2020;137(16):48592.
[18] Akkouche N, et al. *Pyrolysis Polybutadiene Model Including Self-heating and Self-Cooling Effects: Kinetic Study via Particle Swarm Optimization*. Waste Biomass Valoriz 2020;11(2):653–67.
[19] Bernigaud P, Davidenko D, Catoire L. *AP/HTPB Heterogeneous Combustion with revised Kinetics*. Proc Combust Inst 2024;40(1–4):105469.
[20] Bayat Y, Jodar S, Khanlari T. *Synthesis and thermal decomposition kinetics of tri-block copolymer ε-caprolactone / polybutadiene (PCL-PB-PCL); preparation of polyurethane network-based tri-block copolymer*. J Polym Res 2022;29(3):101.
[21] Xuan W, Yan S, Dong Y. *Exploration of Pyrolysis Behaviors of Waste Plastics (Polypropylene Plastic/Polyethylene Plastic/Polystyrene Plastic): Macro-thermal Kinetics and Micro-Pyrolysis Mechanism*. Processes 2023;11(9):2764.
[22] Leung DYC, Wang CL. *Kinetic Modeling of scrap Tire Pyrolysis*. Energy Fuel 1999;13(2):421–7.
[23] Kim E, Dembsey N, Shivkumar S. *Evaluating effects of applying different kinetic models to pyrolysis modeling of fiberglass-reinforced polymer composites*. Fire Mater 2015;39(2):153–73.
[24] Armenise S, et al. *Application of computational approach in plastic pyrolysis kinetic modelling: a review*. React Kinet Mech Catal 2021;134(2):591–614.
[25] LeBlanc, J., *Slow Pyrolysis Experiments for High Yields of Solid Carbon*. 2016, ProQuest Dissertations & Theses.
[26] Bose A, Westmoreland PR. *Predicting Total Electron-Ionization Cross Sections and GC–MS Calibration Factors using Machine Learning*. Chem A Eur J 2020;124(50):10600–15.
[27] National Institute of Standards and, T., NIST Chemistry WebBook – Ionization Energies of Neutral Atoms and Molecules. NIST Standard Reference Database; 2024.
[28] Locaspi A, et al. *Towards a lumped approach for solid plastic waste gasification: Polyethylene and polypropylene pyrolysis*. Waste Manag 2023;156:107–17.
[29] Locaspi A, Pelucchi M, Faravelli T. *Towards a lumped approach for solid plastic waste gasification: Polystyrene pyrolysis*. J Anal Appl Pyrol 2023;171:105960.
[30] Abbas-Abadi MS, et al. *The pyrolysis study of polybutadiene rubber under different structural and process parameters: comparison with polyvinyl chloride degradation*. J Therm Anal Calorim 2022;147(2):1237–49.
[31] Sanglar C, Nguyen Quoc H, Grenier-Loustalot MF. *Studies on thermal degradation of 1-4 and 1-2 polybutadienes in inert atmosphere*. Polym Degrad Stab 2010;95(9):1870–6.
[32] *Active Thermochemical Tables (ATcT)*. Argonne National Laboratory.
[33] Manion, J.A., et al., *NIST Chemical Kinetics Database*, G. National Institute of Standards and Technology, Maryland, 20899-8320, Editor.: https://kinetics.nist.gov/.
[34] Saeys M, et al. *Ab initio group contribution method for activation energies for radical additions*. AIChE J 2004;50(2):426–44.
[35] Nannoolal Y, Rarey J, Ramjugernath D. *Estimation of pure component properties: Part 3. Estimation of the vapor pressure of non-electrolyte organic compounds via group contributions and group interactions*. Fluid Phase Equilib 2008;269(1):117–33.
[36] Nannoolal Y, et al. *Estimation of pure component properties: Part 1. Estimation of the normal boiling point of non-electrolyte organic compounds via group contributions and group interactions*. Fluid Phase Equilib 2004;226:45–63.
[37] Locaspi A, et al. *A lumped kinetic model and experimental investigation of poly (ethylene terephthalate) condensed-phase pyrolysis*. Chem Eng J 2024;500:156955.
[38] Cai J, et al. *Control of thermal cross-linking reactions and the degree of crystallinity of syndiotactic 1,2-polybutadiene*. J Polym Sci B 2005;43(20):2885–97.
[39] Tang J, et al. *Unlocking regioselectivity: steric effects and conformational constraints of Lewis bases in alkyllithium-initiated butadiene polymerization*. Chem Sci 2024;15(48):20493–502.
[40] Tamura S, Gillham JK. *Pyrolysis–molecular weight chromatography–vapor-phase infrared spectrophotometry: an on-line system for analysis of polymers. IV. Influence of cis/trans ratio on the thermal degradation of 1,4-polybutadienes*. J Appl Polym Sci 1978;22(7):1867–84.
[41] Delfour, M., et al., Cationic Polymerization of Dienes. 5. Study of the Polymerization of 1,3-Pentadiene cis/trans Isomers and Evidences of the Origins of the Insoluble Fraction. Macromolecules, 2003. **36**(4): p. 991-998.
[42] Radhakrishnan TS, Rao MR. *Thermal decomposition of polybutadienes by pyrolysis gas chromatography*. J Polym Sci, Polym Chem Ed 1981;19(12):3197–208.
[43] Arisawa H, Brill TB. *Flash pyrolysis of hydroxyl-terminated polybutadiene (HTPB) II: Implications of the kinetics to combustion of organic polymers*. Combust Flame 1996;106(1):144–54.
[44] Sabbe MK, et al. *Modeling the influence of resonance stabilization on the kinetics of hydrogen abstractions*. PCCP 2010;12(6):1278–98.
[45] Chiantore O, et al. *Thermal degradation of polybutadiene, 1. Reactions at temperatures lower than 250°C*. die. Makromol Chem 1989;190(12):3143–52.
[46] Golub MA. *Thermal rearrangements of polybutadienes with different vinyl contents*. J Polym Sci, Polym Chem Ed 1981;19(5):1073–83.
[47] Grassie N, Heaney A. *Thermal reaction of pendent vinyl groups in polybutadiene and copolymers of butadiene and acrylonitrile*. J Polym Sci, Polym Lett Ed 1974;12(2):89–94.
[48] Makhiyanov N. *Determination of configurational isomers in polybutadienes by 1H and 13C NMR spectroscopy*. Polym Sci, Ser A 2012;54(2):69–80.
[49] Rozentsvet VA, et al. *Structural characterization of polybutadiene synthesized via cationic mechanism*. J Polym Sci A Polym Chem 2018;56(4):387–98.
[50] Mochel VD. *Carbon-13 NMR of polybutadiene*. Journal of Polymer Science Part A-1. Polym Chem 1972;10(4):1009–18.
[51] Clague ADH, van Broekhoven JAM, Blaauw LP. *13C Nuclear magnetic Reasonance Spectroscopy of Polydienes*. Microstructure of Polybutadiene Macromolecules 1974;7(3):348–54.
[52] Buszek RJ, et al. *Structure and energetics of hydroxyl-terminated polybutadiene via density functional theory*. Propellants Explos Pyrotech 2023;48(9):e202300123.
[53] Tingfa D, Junfeng L. *Estimation of major volatile products from the first stage of the thermal decomposition of hydroxy-terminated polybutadiene binder*. Thermochim Acta 1991;184(1):81–90.
[54] Brazier DW, Schwartz NV. *The effect of heating rate on the thermal degradation of polybutadiene*. J Appl Polym Sci 1978;22(1):113–24.
[55] McCreedy K, Keskkula H. *Effect of thermal crosslinking on decomposition of polybutadiene*. Polymer 1979;20(9):1155–9.
[56] Chiaverini MJ, et al. *Pyrolysis Behavior of Hybrid-Rocket Solid Fuels under Rapid heating Conditions*. J Propul Power 1999;15(6):888–95.
[57] Qian Y, et al. *A study on the decomposition pathways of HTPB and HTPE pyrolysis by mass spectrometric analysis*. J Anal Appl Pyrol 2023;170:105929.
[58] Lu Y-C, Kuo KK. *Thermal decomposition study of hydroxyl-terminated polybutadiene (HTPB) solid fuel*. Thermochim Acta 1996;275(2):181–91.
[59] Jiang DD, et al. *Thermal decomposition of cross-linked polybutadiene and its copolymers*. Polym Degrad Stab 1999;65(3):387–94.
[60] Williams PT, Besler S. *Pyrolysis-thermogravimetric analysis of tyres and tyre components*. Fuel 1995;74(9):1277–83.
[61] Sircar AK, Lamond TG. *Estimation of butadiene in vulcanized BR and SBR by thermographic analysis*. J Appl Polym Sci 1973;17(8):2569–77.
[62] Lin J-P, et al. *Thermal degradation kinetics of polybutadiene rubber*. Polym Degrad Stab 1996;53(3):295–300.
[63] Karpovych V, et al. *Short timescale high temperature pyrolysis products of hydroxyl-terminated polybutadiene*. Fuel 2023;343:127655.
[64] Brill TB. Chemical Mechanisms at the Burning Surface 1996.
[65] Ranzi E, et al. *Lumping procedures in detailed kinetic modeling of gasification, pyrolysis, partial oxidation and combustion of hydrocarbon mixtures*. Prog Energy Combust Sci 2001;27(1):99–139.
[66] Locaspi A, Frassoldati A, Faravelli T. *Reduced-order condensed-phase kinetic models for polyethylene, polypropylene and polystyrene thermochemical recycling*. Chem Eng J 2024;500:156949.
[67] Luda MP, Guaita M, Chiantore O. *Thermal degradation of polybutadiene, 2. overall thermal behaviour of polymers with different microstructures*. die. Makromol Chem 1992;193(1):113–21.
[68] Chen JK, Brill TB. *Chemistry and kinetics of hydroxyl-terminated polybutadiene (HTPB) and diisocyanate-HTPB polymers during slow decomposition and combustion-like conditions*. Combust Flame 1991;87(3):217–32.
[69] Choi S-S. *Characteristics of pyrolysis patterns of polybutadienes with different microstructures*. J Anal Appl Pyrol 2001;57(2):249–59.
[70] Watson MD, Wagener KB. *Solvent-Free Olefin Metathesis Depolymerization of 1,4-Polybutadiene*. Macromolecules 2000;33(5):1494–6.
[71] Marongiu A, Faravelli T, Ranzi E. *Detailed kinetic modeling of the thermal degradation of vinyl polymers*. J Anal Appl Pyrol 2007;78(2):343–62.
[72] Kinetic Data on Gas Phase Unimolecular Reactions, NSRDS-NBS, Editor; 1964.
[73] Tsang W. *Thermal decomposition of 3,4-dimethylpentene-1, 2,3,3-trimethylpentane, 3,3-dimethylpentane, and isobutylbenzene in a single pulse shock tube*. Int J Chem Kinet 1969;1(2):245–78.
[74] Mehl M, et al. *Oxidation and combustion of the n-hexene isomers: a wide range kinetic modeling study*. Combust Flame 2008;155(4):756–72.
[75] Popov KV, Knyazev VD. *Molecular Dynamics simulation of C–C Bond Scission in Polyethylene and Linear Alkanes: Effects of the Condensed phase*. Chem A Eur J 2014;118(12):2187–95.
[76] Wang K, Villano SM, Dean AM. *Ab initio study of the influence of resonance stabilization on intramolecular ring closure reactions of hydrocarbon radicals*. PCCP 2016;18(12):8437–52.
[77] Popelier G, et al. *Steam cracking of methyl ester: a modeling study on the influence of the hydrocarbon backbone*. J Anal Appl Pyrol 2023;172:105998.
[78] Marongiu A, et al. *Thermal degradation of poly (vinyl chloride)*. J Anal Appl Pyrol 2003;70(2):519–53.
[79] Dente M, et al. In: *Kinetic Modelling of Pyrolysis Processes in Gas and Condensed Phase*, in *Advances in Chemical Engineering*. Academic Press; 2007. p. 51–166.
[80] *Comprehensive Tables*, in *Properties of Polymers (Fourth Edition)*, D.W. Van Krevelen and K. Te Nijenhuis, Editors. 2009, Elsevier: Amsterdam. p. 889-953.
[81] Robert, J.P., *Rapid pyrolysis of polymeric solid propellant binders*. 1976.

[82] Sinha YK, Sridhar BTN, Santhosh M. *Thermal decomposition study of HTPB solid fuel in the presence of activated charcoal and paraffin*. J Therm Anal Calorim 2015;119 (1):557–65.
[83] El-Basuony SA, et al. *Thermokinetic studies of polyurethanes based on hydroxyl-terminated polybutadiene prepolymer*. J Therm Anal Calorim 2018;131(2):2013–9.
[84] Pathak, D.D., *HTPB-Polyurethane: A Versatile Fuel Binder for Composite Solid Propellant*, in *Polyurethane*, D.F. Zafar and E. Sharmin, Editors. 2012, IntechOpen: Rijeka.
[85] Wang K, et al. *Kinetic, thermodynamic and synergistic effects of pyrolysis of natural rubber, styrene-butadiene rubber and butadiene rubber*. Fuel 2024;372:132088.
[86] Ciuta S, et al. *Biomass energy behavior study during pyrolysis process by intraparticle gas sampling*. J Anal Appl Pyrol 2014;108:316–22.
[87] LeBlanc J, Quanci J, Castaldi MJ. *Experimental investigation of reaction confinement effects on coke yield in coal pyrolysis*. Energy Fuel 2016;30(8):6249–56.
[88] Golub MA. *Cis-trans Isomerization in Polybutadiene*. J Polym Sci 1957;25(110): 373–7.
[89] Shirtcliff LD, McClintock SP, Haley MM. Reactions in the conjugated 'ene–ene–yne' manifold: five-membered ring fragmentation and ring formation via coarctate/pseudocoarctate mechanisms. Chem Soc Rev 2008;37(2):343–64.
[90] Bogomolova MN, Zemlyakov DI, Аширов РВ. The influence of the microstructure of low-molecular-weight polybutadiene rubbers on the properties of polydicyclopentadiene. International Polymer Science and Technology 2013;40 (10):11–6.
[91] Liu S, et al. *Rubber pyrolysis: Kinetic modeling and vulcanization effects*. Energy 2018; 155:215–25.